For Reference

NOT TO BE TAKEN FROM THIS ROOM

Ex libris
Universitatis
Albertaensis

QUAECUMQUE VERA

Digitized by the Internet Archive
in 2023 with funding from
University of Alberta Library

https://archive.org/details/Wilson1976_0

THE UNIVERSITY OF ALBERTA

LOCAL ADVECTION ARISING FROM A CHANGE IN SURFACE TEMPERATURE

by

© JOHN DEREK WILSON

A THESIS

SUBMITTED TO THE FACULTY OF GRADUATE STUDIES AND RESEARCH

IN PARTIAL FULFILMENT OF THE REQUIREMENTS FOR THE DEGREE OF

MASTER OF SCIENCE

IN

METEOROLOGY

DEPARTMENT OF GEOGRAPHY

EDMONTON, ALBERTA

FALL, 1976

ABSTRACT

This report is primarily concerned with the modification of the mean temperature profile in the surface boundary layer of the atmosphere caused by a change in surface temperature.

A review of the literature relevant to this subject is given. An experiment is described in which a change in surface temperature was created by irrigation of a small area of grass, and its effect on the airflow measured.

Predictions of an analytical local-advection model were compared with the observed temperature-profile modification. In individual experiments the comparison was inconclusive because of inaccuracy in the experimental data. However, data were averaged over all experiments and there was found to be no significant difference between model and experimental values of the shape factor used for comparison. The model average temperature-gradient stabilisation was found to agree reasonably closely with the experimental averages.

Wind-profile modification was observed to be stronger than that expected from a numerical local-advection model in both several individual experiments and on average.

Several improvements in experimental technique are suggested for consideration by future experimenters.

ACKNOWLEDGEMENTS

I wish to thank Dr. K. D. Hage for his patient and helpful supervision of my study, and his help in execution of the temperature-profile modification experiment.

I am grateful to Dr. J. L. Honsaker, who designed the temperature-sensor network and helped carry out the experiment.

Financial support for the field experiment was provided by the National Research Council. Most of the meteorological field equipment was provided under grants from the National Research Council to the Institute of Earth and Planetary Physics, and by the Water Resources Research Program of the Inland Waters Directorate of Environment Canada.

I wish to thank the Department of Soil Science for permission to use the Ellerslie site, and Dr. R. B. Charlton and Dr. J. A. Toogood for serving on my examining committee.

Finally I wish to express my appreciation for the financial support I have recieved through a Canadian Commonwealth Scholarship.

TABLE OF CONTENTS

Page

ABSTRACT iv

ACKNOWLEDGEMENTS v

TABLE OF CONTENTS vi

LIST OF TABLES viii

LIST OF FIGURES xv

CHAPTER

I INTRODUCTION 1

II THEORETICAL BACKGROUND FOR AN INTERNAL BOUNDARY LAYER 6

- 2.1 Governing Equations 6
- 2.2 Elimination of Velocity as a Variable 8
- 2.3 Power Law Wind and Diffusivity Profiles 9

III ANALYTICAL INTERNAL BOUNDARY LAYER MODELS 12

- 3.1 The Model of Sutton 12
- 3.2 The Microclimate Modification Model of de Vries 14
- 3.3 The Model of Rider, Philip, and Bradley 16
- 3.4 Limitations of the Rider, Philip, and Bradley Model 23

CHAPTER Page

3.5 The Model of Yih 25

3.6 The Shwetz Method 26

3.7 Comparison of Shwetz and Philip Solutions 29

IV NUMERICAL INTERNAL BOUNDARY LAYER MODELS 33

4.1 The Mixing-Length Model of Taylor 33

4.2 Weisman's Extension of the Taylor Model 36

4.3 The Model of Rao, Wyngaard, and Cote 37

4.4 The Model of Novikova 39

V EXPERIMENTAL STUDIES OF TEMPERATURE-PROFILE MODIFICATION 40

5.1 The Experiment of Rider, Philip, and Bradley 40

5.2 The Observations of Dyer and Crawford 43

VI INSTRUMENTATION, SITE, AND PROCEDURE OF THE ELLERSLIE EXPERIMENT 44

6.1 The Temperature Sensors 44

6.2 The Temperature-Sensor Network 46

6.3 The Sonic Anemometer-Thermometer 52

6.4 The Shear Stress Meter and Humidiometer 53

6.5 Retrieval of Data from Magnetic Tape 55

6.6 Experimental Site 56

6.7 Instrument Layout 58

6.8 Experimental Procedure 59

VII TEMPERATURE-PROFILE MODIFICATION 63

CHAPTER Page

7.1 Temperature-Profile Modification Data 63

7.2 Calculation of Parameters Required by the Rider, Philip, and Bradley Model 82

7.3 Comparison of Observed Temperature-Profile Modification with the Rider, Philip, and Bradley Model 85

7.4 Comparison of Model and Experimental Stabilisation 92

VIII MODIFICATION OF THE VELOCITY PROFILE AND THE NET RADIATIVE FLUX 96

8.1 Experimental Wind Profiles 96

8.2 A Simple View of Wind-Profile Modification 103

8.3 Modification of the Net Radiative Flux 105

IX CONCLUSION 108

9.1 Summary of Findings 108

9.2 Recommendations 110

REFERENCES 113

APPENDIX (Nomenclature) 116

LIST OF TABLES

TABLE		Page
7-1	Experimental Conditions	64
7-2	Mean Temperature Differences (°C) and Sample Standard Deviations	65
7-3	Cooling over the Wet Surface (°C) and Sample Standard Deviation	72
7-4	Stabilisation of the Temperature Gradient over the Cool Surface (°K m^{-1})	79
7-5	Wind and Diffusivity Parameters for Input to the RPB Model	84
7-6	Experimental and Model Shape Factors	87
7-7	Mean Values of $\frac{F(z_2) - F(z_1)}{z_2 - z_1}$	93
8-1	Upstream and Downstream Wind Profiles	98

TABLE Page

LIST OF FIGURES

FIGURE Page

1-1 Two-Dimensional Internal Boundary Layer 3

3-1 Shwetz and Philip Solutions for IBL Height 31

6-1 Structure of Temperature Sensors 44

6-2 Sensor Power-Supply 45

6-3 Pattern of Differences 47

6-4 The Experimental Site 57

6-5 Instrument Layout 60

6-6 Photograph Showing Layout 61

7-1 Distribution of Temperature Differences 74

7-2 Cooling over the Wet Surface 76

7-3 Cooling over the Wet Surface under Stable and Unstable Stratification 77

7-4 Stabilisation of the Temperature Gradient over the Cool Surface 81

7-5 Experimental and Model Shape Factor 88

7-6 Model Modification versus u_1/K_1 90

7-7 Model and Experimental Mean Stabilisation 94

FIGURE Page

8-1 Average Deceleration over the Cool Surface 101

CHAPTER 1

INTRODUCTION

The wind transport of any entity, such as heat, momentum, or moisture, which results from surface inhomogeneity on the micrometeorological scale is termed 'local advection'.

Although the phenomenon of local advection has been experienced by man throughout history, it has received considerable attention since about 1950 for several reasons.

It has been realised that local advection is an important aspect of agricultural science. For example, because the microclimate over a finite irrigated area of land is affected by the advection of drier air from upstream unirrigated land, consideration of local advection is necessary for the prediction of water needs for irrigation.

Local advection over smaller distances results in interaction between experimental plots, as pointed out by Rider, Philip, and Bradley (1963) who stated that

> Frequently the dimensions of plots, subjected to different treatments, may be of the order of the range in which advective effects are demonstrably important. It is clear that hetereogeneity between such plots due to differential water treatments, differential aerodynamic roughness or differential radiative balance, may induce significant unwanted interactions between plots. It is clear that the value and applicability of plot experiments to large-scale field experience

> can, in some circumstances, be very greatly enhanced if the presence of advective effects is recognised and appropriate allowances made.

The development and testing of flux and profile laws for the atmospheric boundary-layer lead to increased consideration of the fact that airflow above the ground is very rarely in equilibrium with the surface immediately below it. Surface inhomogeneity in roughness, elevation, temperature, wetness, vegetative cover, soil type, etc., prevents equilibrium because the influence of any disturbance is advected downstream more rapidly than it is propogated vertically, and only in airflow over an extensive horizontally-homogeneous surface will the boundary-layer characteristics be consistent with the surface boundary conditions imposed. Consequently, theoretical and experimental meteorologists began to study disturbed boundary layers, concentrating, in the interests of simplicity, on the two-dimensional internal boundary layer (IBL), which develops within the boundary layer when flow over a uniform surface encounters a step change to new uniform conditions, (see Fig. 1-1.). Although attention has been concentrated on the influence of the surface on turbulence statistics (mean windspeed, turbulent kinetic energy, shear stress, mean temperature) information gained on the effect on airflow of a surface discontinuity is information gained on local advection.

One of the most extensively investigated aspects of airflow over surface inhomogeneity has been the IBL

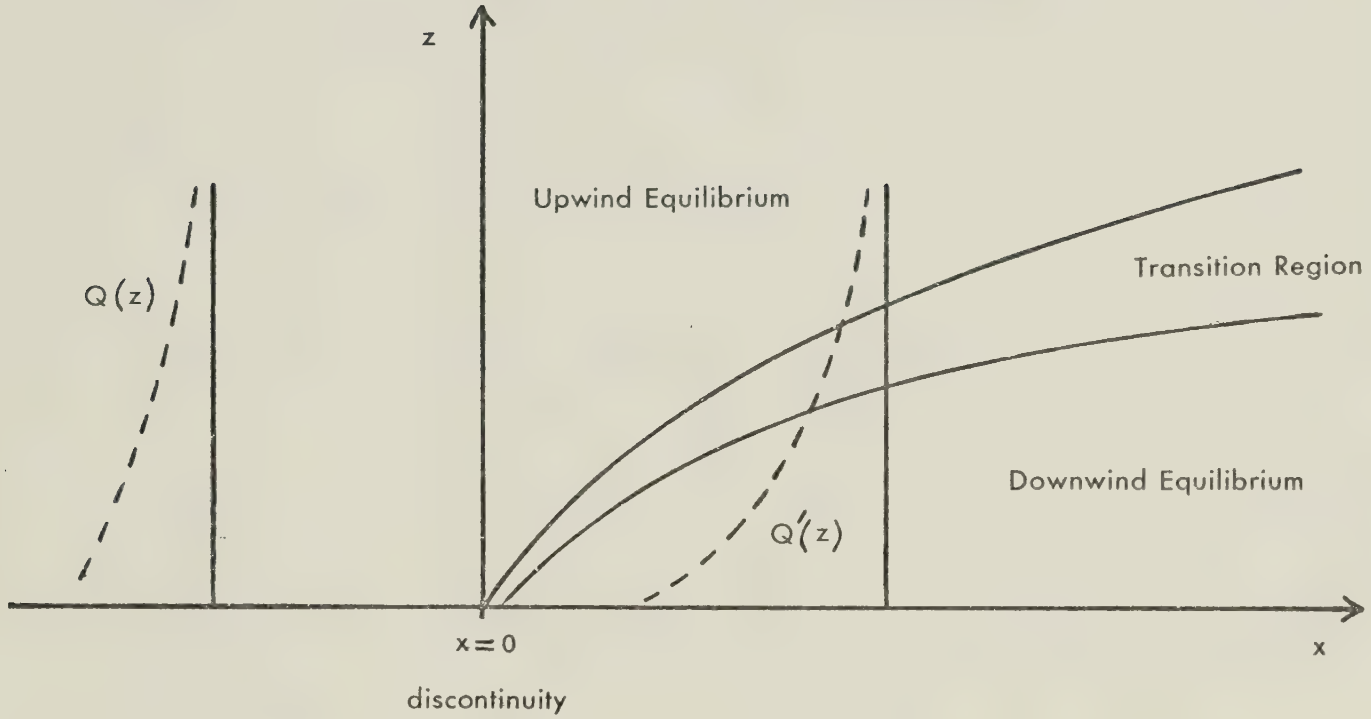

Figure 1-1. Two-dimensional internal boundary layer.

δ (x) height of IBL
Q(z),Q'(z) upwind and downwind profiles of Q

created in flow over a step change in surface roughness. This is probably a consequence of the need to develop criteria for the exposure of anemometers, in order to ascertain that windspeed measurements to be related to the underlying surface are taken within the layer of re-established equilibrium downwind of the nearest discontinuity.

Evaporation from a finite wetted area is another surface discontinuity, or local advection problem that has been widely studied. This problem is very similar to the problem of a surface discontinuity in temperature, if heat is treated as a passive atmospheric property. In nature, both discontinuities usually occur together, because an alteration in surface moisture conditions will alter the partition of available energy into sensible and latent heat fluxes, and thus create a discontinuity in surface temperature. The moisture and temperature fields may be considered to form a field of 'equivalent temperature', defined by

$$\theta_e = T + \left(\frac{L}{\rho c_p}\right)e$$

and under certain circumstances the finite wetted area advection problem may be fully formulated in terms of θ_e. (Symbols used in this report are defined in an appendix. They are only re-defined in the text in cases where this is judged appropriate.)

Sutton (1953) showed that the local evaporation rate decreases with distance from the leading edge, because

of enrichment of the air with vapour. This indicates that surface temperature will not be constant downstream of the leading edge, so that horizontal homogeneity cannot be assumed for either temperature or moisture fields. In addition, because the temperature change may significantly affect the longwave radiation $\epsilon \sigma T_o^4$, and moisture may affect both radiation and soil heat flux, all components of the surface energy balance equation may be changed by the discontinuity.

In the experiment to be reported in this thesis, hereafter referred to as the 'Ellerslie experiment', the primary aim was to study modification of the temperature profile after a step change in surface temperature. However, as the surface temperature change was obtained by irrigating a patch of a large, reasonably uniform grass field, the situation set up was the complex moisture-heat interaction previously discussed.

CHAPTER 2

THEORETICAL BACKGROUND FOR AN INTERNAL BOUNDARY-LAYER

2.1 GOVERNING EQUATIONS

The basic equations governing stratified airflow on the micrometeorological scale are :

The equation of continuity

$$\frac{\partial \rho}{\partial t} + \nabla \cdot \rho \underset{\sim}{v} = 0 \qquad (2.1.1)$$

The momentum equation

$$\frac{d\underset{\sim}{v}}{dt} = -\frac{1}{\rho}\nabla p - g\underset{\sim}{\hat{k}} + \nu\left[\nabla^2 \underset{\sim}{v} + \frac{1}{3}\nabla(\nabla \cdot \underset{\sim}{v})\right] \qquad (2.1.2)$$

The first law of thermodynamics, or 'energy equation'

$$\rho c_v \frac{dT}{dt} + p\nabla \cdot \underset{\sim}{v} = k\nabla^2 T + \rho\phi + \rho c_p \mathcal{R} \qquad (2.1.3)$$

The equation of state

$$p = \rho R T \ . \qquad (2.1.4)$$

Here v, T, ρ, and p are instantaneous values of the velocity vector, temperature, density, and pressure, ϕ is the instantaneous dissipation of kinetic energy into heat, and $\mathcal{R}$ is the rate of heat addition by radiation.

A set of equations describing the mean flow of a turbulent stratified fluid may be derived from the above by

rewriting the instantaneous equations using the Boussinesq approximation, which assumes that density fluctuations are negligible unless multiplied by gravity, then splitting the flow into mean and fluctuating components using the Reynolds averaging convention. This procedure is demonstrated by Plate (1971).

The resulting equations for the mean flow are, using the summation convention :

The equation of continuity

$$\frac{\partial u_i}{\partial x_i} = 0 \tag{2.1.5}$$

The momentum equation

$$\frac{du_i}{dt} = -\frac{1}{\rho_0}\frac{\partial p}{\partial x_i} + g\frac{T}{T_0}\delta_{3i} - \overline{u_j' \frac{\partial u_i'}{\partial x_j}} \tag{2.1.6}$$

The thermodynamic equation

$$\frac{dT}{dt} = -\frac{\partial}{\partial x_j}\overline{u_j' T'} \tag{2.1.7}$$

where a prime denotes a fluctuating quantity and all other quantities are now mean values. T_0 and ρ_0 are values for a hypothetical reference state with adiabatic lapse rate and hydrostatic equilibrium.

In order to obtain these results viscous friction, molecular heat transfer and radiative flux divergence have been neglected.

Equations (2.1.5)-(2.1.7), augmented by such additional conservation equations as are necessary to describe a particular problem, are the basis for the

mathematical formulation of the internal boundary-layer problem. They apply to small-scale motion in the atmospheric boundary layer regardless of the presence of surface inhomogeneity, and are therefore valid inside, outside, and on the boundary of any IBL.

2.2 Elimination of Velocity as a Variable

In the analytical models to be discussed in Chapter 3, the number of equations is reduced and the problem simplified by the use of pre-specified velocity profiles, which are assumed to describe the flow both inside and outside the IBL. Through this approximation the variable $\underset{\sim}{v}$ becomes simply a parameter in the IBL equations, and the momentum and continuity equations are no longer required. Given a realistic approximation for the velocity profile, the approach should be satisfactory for the description of any IBL set up by a discontinuity which is not likely to affect the velocity profile (e.g., step introduction of a completely passive contaminant). However in other cases , modification of the velocity profile is one of the important effects of the discontinuity (e.g., change in roughness) and a full formulation of the problem, including the momentum equation, is desirable.

2.3 Power Law Windspeed and Diffusivity Profiles

In the theoretical models of local advection which will be described in Chapter 3 the wind profile is commonly approximated by the power law

$$u = u_1\left(\frac{z}{z_1}\right)^m \quad , \quad m \geqslant 0 \tag{2.3.1}$$

and the diffusivity by

$$K = K_1\left(\frac{z}{z_1}\right)^n \quad . \tag{2.3.2}$$

The true wind profile has been found to have the curvature

$$\frac{\partial^2 u}{\partial(\ln z)^2} = z\frac{\partial u}{\partial z} + z^2\frac{\partial^2 u}{\partial z^2}$$

>0 for stable stratification

=0 for neutral stratification

<0 for unstable stratification

(see Sutton (1953)).

The restrictions placed on m are then

$m^2>0$ stable

$m^2=0$ neutral

$m^2<0$ unstable stratification.

In order that u increase with height, m>0 is required. It can thus be seen that the power law fit to unstable and neutral wind profiles is not very accurate.

The vertical fluxes in the lower atmosphere are measured to be approximately constant under the following conditions:

(1) Steady flow

(2) Horizontal uniformity in all properties

(3) Zero radiative flux divergence.

Under such conditions a relation known as 'Schmidt's conjugate power law' holds, i.e.,

$$n=1-m$$

where n is the exponent in the power law for momentum diffusivity. If this law holds, measurement of the wind profile gives an approximation to the momentum diffusivity profile, and through assumed relations between K_m , K_T , and K_e , an approximation to the other diffusivities.

In the models to be described in this thesis, interest is in the wind profiles in the lowest 2 m of the atmosphere, where stability effects are expected to be unimportant, and the wind profiles should show the shape characteristic of neutral stability regardless of stratification. To represent a neutral profile we require

$\ln z \propto z^m$, say $m = [\ln(\ln z)] / \ln z$.

From this formula, m is undefined at z=0 or z=1, has the value 0.36 at z=10, and decreases with increasing height thereafter.

The value of m for neutral conditions is commonly chosen as $\frac{1}{7}$, a figure originally based on wind tunnel experiments. However, this value is most successful in a range of heights of 2 to 4 m, whereas in the Ellerslie experiment m was chosen to best represent the wind profile below 2 m, and values of around 0.26 were required.

Under stable stratification m is expected to increase towards unity, while for unstable stratification it should decrease. However, as has been noted, very close to the ground the wind profile is always approximately neutral, and in the Ellerslie experiment values of m were always between 0.24 and 0.30. These values agree well with those reported by Morgan, Pruitt, and Lourence (1971).

Use of the power law relations and Schmidt's conjugate power law is most convenient in analytical formulations, but it must be remembered that the technique is only an approximation.

CHAPTER 3

ANALYTICAL INTERNAL BOUNDARY-LAYER MODELS

3.1 The Model of Sutton

The steady-state two-dimensional diffusion of heat in incompressible turbulent flow may be described by the equation

$$u \frac{\partial T}{\partial x} = \frac{\partial}{\partial z}\left(K_T \frac{\partial T}{\partial z}\right). \qquad (3.1.1)$$

This equation is obtained from the thermodynamic equation for turbulent flow (2.1.7) by modelling the vertical heat flux using the mixing-length approach

$$-\overline{\omega' T'} = K_T \frac{\partial T}{\partial z} \quad . \qquad (3.1.2)$$

Molecular heat transfer is not included, and the divergence of the horizontal turbulent heat flux has been neglected.

Equation (3.1.1) may be generalised to describe the two-dimensional diffusion of any passive property in incompressible flow,

$$u \frac{\partial \theta}{\partial x} = \frac{\partial}{\partial z}\left(K_\theta \frac{\partial \theta}{\partial z}\right) \qquad (3.1.3)$$

where θ is the concentration of the atmospheric property under consideration.

Sutton (1953) gave a solution of (3.1.3) subject

to the boundary conditions:

$$\lim_{z \to 0} \theta(x,z) = \theta_1 - \theta_0 \quad \text{for } x \geqslant 0$$

$$\lim_{x \to 0} \theta(x,z) = 0 \quad \text{for } z > 0$$

$$\lim_{z \to \infty} \theta(x,z) = 0 \quad \text{for } x \geqslant 0$$

If θ is regarded as a temperature difference $T-T_0$ Sutton's solution gives the temperature in the IBL that is formed when neutrally-stratified air at temperature T_0 encounters a step jump in surface temperature to a new surface temperature T_1.

Sutton used power-law expressions for wind and diffusivity. He related the two profiles through an approximation for the Lagrangian autocorrelation coefficient to obtain

$$u = u_1 \left(\frac{z}{z_1}\right)^{\frac{n}{2-n}}$$

$$K = a \left(\frac{z}{z_1}\right)^{\frac{2(1-n)}{2-n}}$$

where a is a known function of n, z_1 and kinematic viscosity; z_1 is the reference height. For neutral conditions, n=0.25.

The solution for temperature within the IBL is

$$T(x,z) - T_0 = (T_1 - T_0)\left\{1 - \frac{1}{\pi} \sin\frac{2\pi}{2+n}\, \Gamma\left(\frac{2}{2+n}\right) \Gamma_i\left[b\, \frac{z^{\left(\frac{2+n}{2-n}\right)}}{x}, \frac{n}{2+n}\right]\right\}$$

where b is a known function of u_1, z_1, n, ν and Γ_i is the incomplete gamma function,

$$T_i(\theta, p) = \int_0^\theta x^{p-1} e^{-x} \, dx \, .$$

It is interesting to note that this solution is very similar in form to that obtained by Philip (1959) , (see Section 3.3), for the same problem, probably differing only in the choice of power-law coefficients.

3.2 The Microclimate Modification Model of de Vries

De Vries (1959) presented a theory of the influence of sustained irrigation on the energy balance and climate near the ground.

The variables considered were

$$\theta = T_i - T_d$$

$$q = q_i - q_d$$

where 'i' refers to irrigated land values and 'd' refers to dry land values. Guided by measurements, de Vries neglected time changes in θ and q, which he states are small compared to the spatial changes. The diffusion equation, (3.1.3), is the basis of the analysis, and all variables are considered to be averages over several days.

The wind and diffusivity profiles are represented by

$$u = u_0 \left(1 + \frac{z}{z_1}\right)^m$$

$$K = K_0 \left(1 + \frac{z}{z_1}\right)$$

and it is assumed that these profiles are unaltered as the air flows over the irrigated surface.

The boundary conditions are :

(i) $\lim_{z\to\infty} q(x,z)=0$

$\lim_{z\to\infty} \theta(x,z)=0$

(ii) A simplified time-averaged energy balance condition at the surface for temperature

$$A_i - A_d = -L\rho_w I - \epsilon\sigma\left(T_{od}^4 - T_{oi}^4\right)$$

(iii) A water balance equation at the surface

$$-\rho\left(K_e \frac{\partial q}{\partial z}\right)_{z=0} = \rho_w I$$

where I is the irrigation rate, assuming no runoff.

The solution is complicated, and Rider, Philip, and Bradley (1963) stated that numerical solutions are very laborious to calculate.

De Vries tested his model by setting up four climatic recording stations, one over unirrigated land , the other three up to six kilometers downwind over irrigated pasture. Starting with the meteorological data for the dry land, averaged over periods of a few days or longer, the average temperature and moisture profiles over the irrigated area were calculated as functions of downwind distance. The predictions were proven to be reasonably accurate. The standard errors in the upstream-downstream differences were 0.3°C (in temperature) and 0.7°C (in dewpoint). Typical differences were:

$\Delta T(0\text{ cm}) = 5°C$

$\Delta T(125\text{ cm}) = 1°C$

$\Delta T_D(0\text{ cm}) = 6°C$

$\Delta T_D(125\text{ cm}) = 1°C$

The de Vries model also provides a means of estimating the potential evaporation rate and thus the water needs of irrigated crops.

3.3 The Model of Rider, Philip, and Bradley

Philip (1959) presented a theory of local advection in which (3.1.3) is solved for concentration, flux, and radiation boundary conditions.

The power-law equations (2.3.1) and (2.3.2) are used for windspeed and diffusivity[1]. Through this approach the variable u becomes simply a pre-specified parameter in the IBL equations and the momentum equation is no longer required. The theory is developed for any m and n, but in this discussion it will be limited to the case where Schmidt's conjugate power-law holds, n=1-m .

Philip's method is as follows. The transformation

$$\eta = \frac{u_1 \, z_1^{\,1-2m}}{(1+2m)^2 \, K_1} \quad \frac{z^{1+2m}}{x} \tag{3.3.1}$$

reduces (3.1.3) and the power-law equations to the equation

$$\frac{d^2\theta}{d\,\eta^2} + \frac{d\theta}{d\eta}\left(1 + \frac{1+m}{1+2m}\,\eta^{-1}\right) = 0 \,. \tag{3.3.2}$$

It is straighforward to integrate (3.3.2) twice to obtain the general solution for the concentration of θ,

---

[1] In fact, Philip (1959) and Rider, Philip, and Bradley (1963) used power-law forms without the z_1 which is included in (2.3.1) and (2.3.2). The forms given in this report are dimensionally correct.

$$\theta(\eta) = B\int_0^{\eta} \eta^{-\left(\frac{1+m}{1+2m}\right)} e^{-\eta} \, d\eta + C \quad . \tag{3.3.3}$$

It is interesting to note that the parameters u_1 and K_1 affect the solution only through their ratio u_1/K_1, which appears in η.

Constants B and C are evaluated by using the boundary conditions, which may be of three basic types:

(i) Concentration Type

$\lim_{\eta\to\infty} \theta(\eta)=\theta_0$ or $\theta_0(z)$, i.e. $\theta=\theta_0$ or $\theta_0(z)$ when $x=0, z>0$.

$\theta(\eta)=\theta_1(x)$ when $\eta=0$, i.e. when $x\geq 0$ and $z=0$.

(ii) Flux Type

$\lim_{\eta\to\infty} \theta(\eta)=\text{constant}$, i.e. $\theta=\text{constant}$ when $x=0, z>0$.

$\phi = \phi_0(x)$ when $x\geq 0$ and $z>0$,

where

$$\phi = -K\frac{\partial\theta}{\partial z}$$

$$\phi_0 = \lim_{z\to 0}\left(-K\frac{\partial\theta}{\partial z}\right).$$

(iii) Radiation Type

This type of boundary condition involves a linear combination of concentration and flux conditions at $\eta=0$ (i.e. At $x\geq 0$, $z=0$).

Now, for example, if one considered neutrally-stratified air in equilibrium flow over a surface at temperature T_0 passing onto a surface with constant temperature T_1, the relevant boundary conditions would be of the concentration type:

$\lim_{\eta\to\infty} T=T_0$, i.e. $T=T_0$ when $x=0, z>0$

$T=T_1$ for $\eta=0$ i.e. $T=T_1$ when $x\geq 0$, $z=0$.

Application of these boundary conditions to (3.3.3) gives the solution for air temperature downstream from the discontinuity,

$$T(x,z)-T_0=(T_1-T_0)\left[1-I\left(\eta,-\frac{1+m}{1+2m}\right)\right] \tag{3.3.4}$$

where $I(\eta,p)$ represents the incomplete gamma function ratio

$$I(\eta,p)=\int_0^{\eta}\eta^{p}e^{-\eta}\,d\eta\Big/\int_0^{\infty}\eta^{p}e^{-\eta}\,d\eta \quad .$$

Philip gave the following expression for evaluation of the incomplete gamma function ratio:

$$I\left(\eta,-\frac{1+m}{1+2m}\right) \tag{3.3.5}$$

$$=\frac{\eta^{1/\beta}}{\Gamma\left(\frac{\beta+1}{\beta}\right)}\left[1-\frac{\eta}{\beta+1}+\frac{\eta^{2}}{2!\,(2\beta+1)}-\frac{\eta^{3}}{3!\,(3\beta+1)}+\cdots\right]$$

where

$$\beta=\frac{1+2m}{m}$$

and Γ is the gamma function. The series converges rapidly so that I can be computed quickly to any desired accuracy.

Flux boundary conditions are treated by Philip as follows.

Rewrite (3.1.3) using the flux-gradient relation

$$\phi=-K\frac{\partial\theta}{\partial z}$$

to obtain

$$\frac{\partial\theta}{\partial x}=-\frac{1}{u}\frac{\partial\phi}{\partial z} \quad .$$

Differentiate with respect to z to obtain

$$\frac{1}{K}\frac{\partial \phi}{\partial x} = \frac{\partial}{\partial z}\left(\frac{1}{u}\frac{\partial \phi}{\partial z}\right) .$$

This equation is analogous to (3.1.3), with

θ replaced by ϕ

n replaced by -m

m replaced by -n (=m-1)

u replaced by K^{-1}

K replaced by u^{-1}.

It is solved by the method of solution of (3.1.3) to obtain

$$\phi = B'\int_0^{\eta'} \eta^{-\left(\frac{m}{2m-1}\right)} e^{-\eta}\, d\eta + C'$$

where

$$\eta' = \frac{K_1^{-1}\, z_1^{2m-1}}{(1+2m)^2\, u_1^{-1}} \quad \frac{z^{2m-1}}{x} .$$

The flux boundary conditions may then be applied.

Rider, Philip, and Bradley (1963) considered the steady-state two-dimensional diffusion of heat and moisture in the lower atmosphere for the case of a step change in surface conditions.

The equations are

$$u\frac{\partial T}{\partial x} = \frac{\partial}{\partial z}\left(K_T \frac{\partial T}{\partial z}\right) \qquad (3.3.6)$$

$$u\frac{\partial e}{\partial x} = \frac{\partial}{\partial z}\left(K_e \frac{\partial e}{\partial z}\right) \qquad (3.3.7)$$

with

$$u = u_1\left(\frac{z}{z_1}\right)^m$$

$$K_T = K_e = K = K_1\left(\frac{z}{z_1}\right)^n .$$

The upstream boundary condition is

$$T = T(0,z) \quad \text{and} \quad e = e(0,z) \quad \text{for} \quad x = 0,\ z \geq 0 . \qquad (3.3.8)$$

The downstream surface boundary condition must be supplied by the equation for energy balance at the surface,

$$(1-r)R_s + R_a - \epsilon\sigma T^4(x,0) + G = A + L\rho_w E \qquad (3.3.9)$$

and an equation for the availability of water for evaporation at the surface,

$$e_0 = e_s(T(x,0)) \quad \text{for} \quad x > 0,\ z = 0 . \qquad (3.3.10)$$

(3.3.10) assumes that water is freely available at the surface.

By defining equivalent temperature

$$\theta_e = T + (L/\rho c_p)e$$

and a new variable

$$\Theta_e(x,z) = \theta_e(x,z) - \theta(0,z)$$

(3.3.6) and (3.3.7) can be written

$$u\frac{\partial \Theta_e}{\partial x} = \frac{\partial}{\partial z}\left(K\frac{\partial \Theta_e}{\partial z}\right) .$$

The upstream boundary condition becomes

$\Theta_e = 0$ for $x=0, z\geq 0$.

Equations (3.3.9) and (3.3.10) for the downstream boundary condition are linearized to obtain a boundary

condition on the surface flux of Θ_e.

The problem is then soluble by the method of Philip, and a most important conclusion of Rider, Philip, and Bradley is that, to a high degree of accuracy, the solution is identical to that which would be obtained by replacing the downstream boundary condition, (3.3.9) and (3.3.10), by the conditions of constant surface temperature T_1 and constant absolute humidity $e_1 = e_s(T_1)$ for $x>0$. This is equivalent to the assumption that the quantities

$$(1-r)R_s + R_a - \epsilon\sigma T^4(x,0) + G$$

and
$$A + L\rho_w E$$

are independent of x. Therefore it is concluded that the primary influence of the discontinuity in moisture and temperature conditions is a change in the energy partition between sensible and latent heat flux.

In the light of these conclusions, Rider, Philip, and Bradley simplified their approach to the problem of modification of the mean flow by a step change in surface conditions. By defining

$$T^* = T(x,z) - T(0,z)$$

and making use of the fact that there is horizontal uniformity upstream from the discontinuity, the problem may be rewritten as the solution of

$$u\frac{\partial T^*}{\partial x} = \frac{\partial}{\partial z}\left(K\frac{\partial T^*}{\partial z}\right)$$

subject to the concentration boundary conditions

$$T^* = 0 \qquad \text{for} \quad x = 0,\ z \geqslant 0$$

$$T^* = T_1 - T_0 \quad \text{for} \quad x > 0, \; z = 0 .$$

The solution is obtained by specifying the general variable θ in (3.3.3) equal to T^*, with

$$\eta_T = \frac{u_1 Z_1^{1-2m}}{(1+2m)^2 K_1} \; \frac{Z^{1+2m}}{x}$$

and using the boundary conditions on T^* to evaluate the constants B and C. The result is the equation

$$T(x,z) - T(0,z) = (T_1 - T_0)\left[1 - I\left(\eta_T, -\frac{1+m}{1+2m}\right)\right]. \quad (3.3.11)$$

An analogous procedure leads to the equation for modification of the absolute humidity

$$e(x,z) - e(0,z) = (e_1 - e_0)\left[1 - I\left(\eta_e, -\frac{1+m}{1+2m}\right)\right]. \quad (3.3.12)$$

Rider, Philip, and Bradley gave a method of determining

$\Delta T_0 = T_1 - T_0$ and $\Delta e_0 = e_1 - e_0$

from K_e/K_T, m, e(0,0) and T(0,0).

With measurements of

(i) upstream wind, temperature, and humidity profiles

(ii) upstream surface temperature and surface absolute humidity

(iii) the diffusivities, which may be calculated, for example, from the relevant fluxes and gradients

one can, under the assumptions of the theory, calculate downstream profiles of temperature and absolute humidity.

3.4 Limitations of the Rider, Philip, and Bradley Model

There are many limitations to the model of Rider, Philip, and Bradley, (hereafter referred to as the 'RPB model').

As has been discussed, (Section 2.3), the power-law profiles are generally a poor approximation to the real profiles. Furthermore, it is assumed that the wind and diffusivity profiles are unaltered by the change in the surface boundary conditions. While IBL situations in which this approximation could be accurate are conceivable, the case of a discontinuity in surface temperature and wetness is not such a case, and it is not likely that heat can accurately be treated as a passive contaminant.

That neglect of thermal stratification is an important weakness in the model is confirmed by the numerical models of Taylor (see Section 4.1) and Rao, Wyngaard, and Cote (see Section 4.3). Taylor states that 'the importance of changes in thermal stability in the leading-edge problem should not be underestimated'.

Downstream of any discontinuity there will exist horizontal gradients, so that the fluxes will not be constant with height and Schmidt's conjugate power-law connecting windspeed and diffusivity will no longer be valid. It has been pointed out that the RPB model is not restricted to the case where Schmidt's conjugate power-law is valid. However, in all applications of the model discussed in this report the conjugate power-law has been

used, and the weakness in this approximation must be remembered.

A further criticism of the RPB model concerns the assumption, embodied in boundary condition (3.3.10), that water is freely available at the downstream surface and that the absolute humidity at the surface is the saturation value. The numerical model of Rao, Wyngaard, and Cote showed that the assumption of saturation at the surface overpredicts the modification in the IBL.

Finally it should be noted that the use of diffusivities is a device by which flux terms (covariances) arising in the boundary-layer equations (see Section 2.1) are related to vertical gradients. These relationships are known as 'K-theory' or the 'mixing-length model' and, since they define the diffusivities, their accuracy in expressing the fluxes is limited by the accuracy with which the diffusivities are specified.

3.5 The Model of Yih

Yih (1952) found exact solutions to the general two-dimensional diffusion equation (3.1.3) using power-law expressions (2.1.3)-(2.1.4) for windspeed and diffusivity. The method used was dimensional analysis.

When the diffusing entity is regarded as temperature and the power-law equations are specialised to the case $n=1-m$, Yih's solution is the same as that of Philip (Section 3.3) for the flow of neutrally-stratified air from a surface at constant temperature T_0 onto a surface at constant temperature T_1. The two authors have solved the same set of equations subject to the same boundary conditions by completely different methods and obtained identical solutions, although this is not clear because of difference in nomenclature.

Yih does not give a solution applicable to the case of non-neutral upstream flow.

3.6 The Shwetz Method

Shwetz (1949) presented a method for approximating the solutions to several boundary-layer problems. His method has been summarised by Panchev, Donev, and Godev (1971), and may be applied to stationary turbulent diffusion as follows.

Multiply the two-dimensional diffusion equation, (3.1.3), by K(z) and introduce the new variables

$$\eta = \int_0^z \frac{dz}{K(z)} \qquad (3.6.1)$$

$$\phi(\eta) = u(\eta)\, K(\eta)$$

to obtain

$$\phi(\eta) \frac{\partial \theta}{\partial x} = \frac{\partial^2 \theta}{\partial \eta^2} \quad . \qquad (3.6.2)$$

Let the boundary conditions be

(i) $\theta=1$ at $z=0, x>0$

(ii) $\theta=0$ at $x=0$ for all z ('θ-less' upstream flow)

(iii) $\lim_{z \to \infty} \theta=0$

corresponding to a step at x=0 from zero concentration of θ to concentration unity at the surface. These boundary conditions will necessitate the growth of an IBL, and the edge of this IBL is defined by $\theta(x, \delta)=0$.

The value of θ within the IBL is now given by (3.6.2) subject to the boundary conditions

$$\theta(x,\delta) = 0 \quad , \; \theta(x,0) = 1 \quad . \qquad (3.6.3)$$

The Shwetz method is to find the solution with the help of successive approximations

$$\theta = \theta_0 + \theta_1 + \theta_2 + \ldots$$

where the individual contributions satisfy approximate forms of (3.6.2),

$$\frac{\partial^2 \theta_0}{\partial z^2} = 0 \quad , \frac{\partial^2 \theta_1}{\partial z^2} = \phi\,\theta_0 \quad , \frac{\partial^2 \theta_2}{\partial z^2} = \phi\,\theta_1 \; , \cdots \qquad . \; (3.6.4)$$

(Shwetz gives no theoretical argument indicating that the above series approximation for θ will be convergent. However, in his paper he shows that accurate solutions to many boundary-layer problems are obtained by this method even when the series is terminated after the second term.)

The first-order solution is obtained from (3.6.4) and boundary conditions (3.6.3) as

$$\theta_0 = 1 - \eta/\delta \quad .$$

The second-order solution is obtained using (3.6.4) for $\frac{\partial^2 \theta_1}{\partial \eta^2}$, integrating twice, and adding θ_0 to give for θ the expression

$$\theta = 1 - \frac{\eta}{\delta} + \left(\frac{\partial \delta}{\partial x}\right)\left(\frac{1}{\delta^2}\right)\int_0^{\eta}\left(\int_0^{\beta} y\,\phi(y)\,dy\right)d\beta + \left(\frac{\partial \theta_1}{\partial \eta}\right)_0 \eta + \left(\theta_1\right)_0 \quad . \qquad (3.6.5)$$

Application of the boundary conditions (3.6.3) gives

$$\left(\theta_1\right)_{z=0} = 0 \quad ,$$

$$\left(\frac{\partial \Theta_1}{\partial \eta}\right)_{z=0} = \frac{-1}{\delta^3} \frac{\partial \delta}{\partial x} \int_0^{\delta} \left(\int_0^{\beta} y \phi(y)\, dy \right) d\beta \quad . \tag{3.6.6}$$

The double integrals in (3.6.5)-(3.6.6) may be simplified by exchange of the order of integration. $\frac{\partial \delta}{\partial x}$ is evaluated by stipulating that

$$\left(\frac{\partial \Theta}{\partial \eta}\right)_{\eta=\delta} = 0 \tag{3.6.7}$$

and the equation for the growth of the IBL is

$$\frac{\partial \delta}{\partial x} \int_0^{\delta} y^2 \phi(y)\, dy = \delta^2 \quad . \tag{3.6.8}$$

The second-order solution for the concentration in the IBL is then found to be

$$\Theta = 1 - \eta (T_1 - J_1)/J_2 \quad - \quad T_2/J_2 \tag{3.6.9}$$

where $T_1 = \int_0^{z} y \phi(y) dy$

$J_1 = \int_0^{\delta} y \phi(y)\, dy$

$T_2 = \int_0^{z} y^2 \phi(y)\, dy$

$J_2 = \int_0^{\delta} y^2 \phi(y)\, dy$.

Equation (3.6.8) for the growth of the IBL may be rewritten

$$\frac{\partial \delta}{\partial x} J_2 = \delta^2 \quad . \tag{3.6.10}$$

3.7 Comparison of Shwetz and Philip Solutions

Write u and K as power-law functions of z,

$$u = u_1 \left(\frac{z}{z_1}\right)^m \qquad K = K_1 \left(\frac{z}{z_1}\right)^n \quad .$$

Assuming n=1-m (constant flux layer), the Shwetz parameters become

$$\eta = b^{-1} z^m$$

$$J_1 = \frac{u_1 b^{\beta-1}}{z_1^m (1+2m)} \delta^\beta$$

$$T_1 = \frac{u_1 b^{-1}}{z_1^m (1+2m)} z^{1+2m}$$

$$J_2 = \frac{u_1 b^{\beta-1}}{z_1^m (1+3m)} \delta^{\beta+1}$$

$$T_2 = \frac{u_1 b^{-2}}{z_1^m (1+3m)} z^{1+3m}$$

where

$$b = K_1 m z_1^{m-1}$$

$$\beta = \frac{1+2m}{m} \quad .$$

The height of the IBL, given by (3.6.11), is

$$z_\delta = (b\delta)^{1/m} = x^{1/1+2m} \times \left[\text{Function of } (m, u_1, K_1, z_1)\right]. \quad (3.7.1)$$

Now for any set of u_1, m, K_1, and z_1, $\theta(x,z)$ and $z_\delta(x)$ as given by the Shwetz solution may be calculated.

The solution given by Philip (see Section 3.3) for the case of θ-less upstream flow encountering a step jump at the surface from $\theta=0$ to $\theta=1$ is

$$\theta(x,z) = 1 - I\left(\xi\,,\ -\frac{1+m}{1+2m}\right) \qquad (3.7.2)$$

where

$$\xi = \frac{u_1\, z_1^{\,1-2m}}{K_1\,(1+2m)^2}\quad \frac{z^{\,1+2m}}{x} \quad .$$

The two solutions will now be compared in several different flow situations. It must be borne in mind that the height of the IBL will depend on its definition. For the Shwetz method, the definition is (3.6.7). For the Philip method, unless otherwise specified, IBL height will be defined to be the height at which the value of θ has decreased to 5 percent of its surface value of 1.0.

In the Ellerslie experiment the mean value of m over all trials was 0.26 with a range of 0.24 to 0.30 . The Shwetz and Philip solutions will be compared for m=0.26, with a variety of values of the diffusivity.

Under forced convection conditions $K_T = K_m = ku_* z$ where for a grassy surface with individual blades 5 cm in length, $u_* = 40$ cm² s⁻¹. This gives $K_1 = K_m(30\text{cm}) = 480$ cm² s⁻¹.

For the Ellerslie data a considerable range of K_1 values has been calculated, from 130 cm² s⁻¹ up to 830 cm² s⁻¹ . The corresponding values of u do not vary greatly, and their average is 180 cm s⁻¹ .

Figure 3.1 compares the Shwetz and Philip solutions. Two curves are given for the Philip model in the

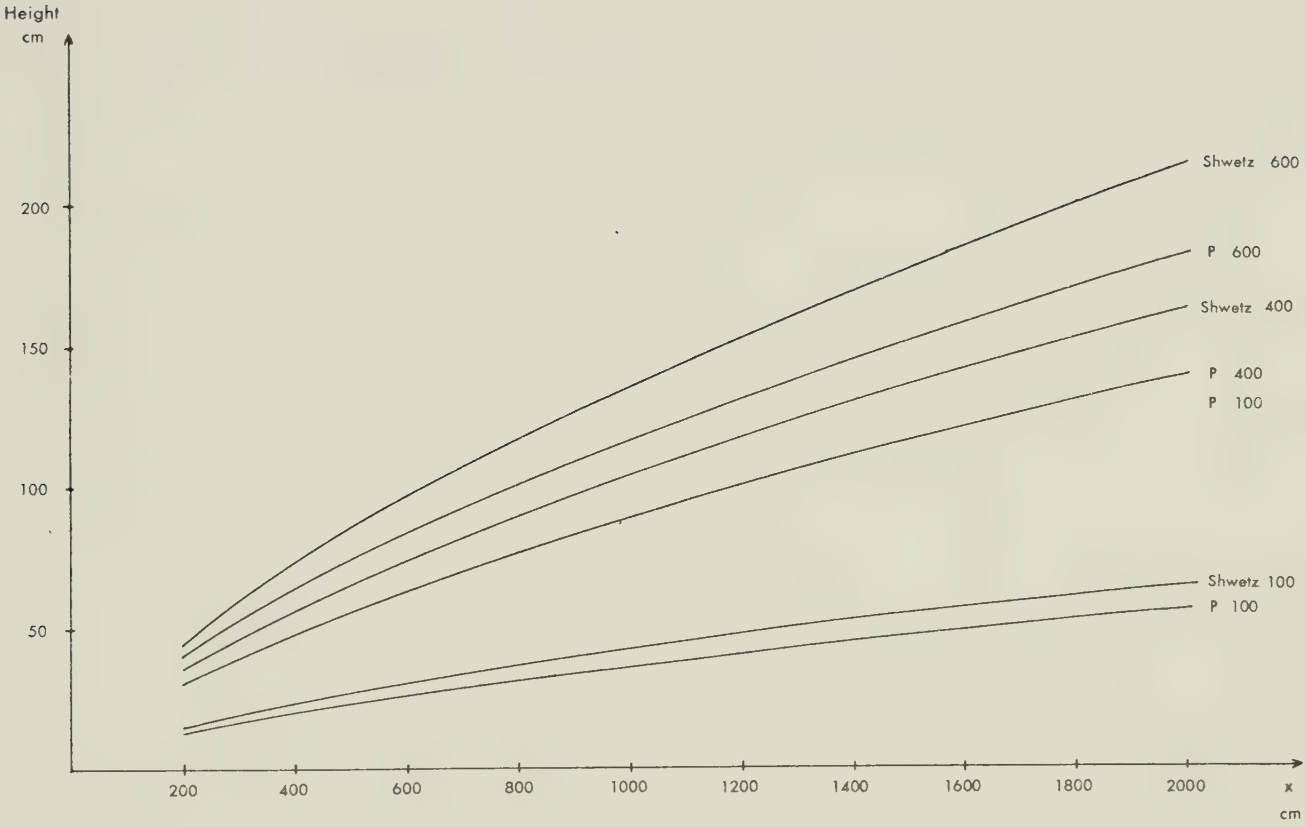

Figure 3-1. Shwetz and Philip Solutions for IBL Height.

case $K_1 = 100$ cm^2 s^{-1}, the higher being the case in which IBL height is defined as the height at which θ drops to 0.1 percent of its surface value of 1.0. It can be seen that the height of the IBL depends quite strongly on the criterion used to define it.

Although (3.7.1) and (3.7.2) apply to the artificial problem of 'θ-less' upstream flow encountering a step jump at the surface from $\theta=0$ to $\theta=1$, they were found to be useful in interpretation of the experimental temperature-profile modification data, because they give some idea of possible IBL height for given fetch.

CHAPTER 4

NUMERICAL INTERNAL BOUNDARY-LAYER MODELS

4.1 The Mixing-Length Model of Taylor

Taylor (1970) presented a numerical model of airflow over a surface discontinuity in roughness, heat flux, or temperature. The model is restricted to two-dimensional steady flow.

The following equations were used for the mean motion, and were assumed to be valid upstream and downstream from the discontinuity:

(i) The equation of continuity (2.1.5)

(ii) A horizontal momentum equation derived from (2.1.6) by neglecting the horizontal pressure gradient and $\frac{\partial}{\partial x}\overline{u'^2}$ terms

$$u\frac{\partial u}{\partial x} + \omega\frac{\partial u}{\partial z} = \frac{\partial u_*^2}{\partial z}$$

(iii) A thermodynamic equation derived from (2.1.7) by neglecting horizontal heat fluxes

$$\rho c_p\left(u\frac{\partial T}{\partial x} + \omega\frac{\partial T}{\partial z}\right) = -\frac{\partial A}{\partial z} \quad .$$

The fluxes were modelled using the Businger-Dyer forms for the Monin-Obukhov similarity functions; thus, for example, the $-\overline{u'w'}$ or u_*^2 term is specified by the gradient

$\frac{\partial u}{\partial z}$ given the appropriate similarity function. The formulation is, therefore

$$\frac{\partial u}{\partial z} = \frac{u_*}{k(z+z_0)} \phi_m\left(\frac{z}{L}\right) \tag{4.1.1}$$

$$\frac{\partial T}{\partial z} = \frac{T_*}{k(z+z_0)} \phi_h\left(\frac{z}{L}\right) \tag{4.1.2}$$

where

$$T_* = \frac{-1}{u_*} \frac{A}{\rho c_p}$$

and

$$L = \frac{-u_*^3}{k\frac{g}{T_0}\left(\frac{A}{\rho c_p}\right)} .$$

For neutral and unstable conditions,

$$\phi_m = \left(1 - 16.0 \frac{z+z_0}{L}\right)^{-1/4} \tag{4.1.3}$$

$$\phi_h = \phi_m^2$$

while for stable conditions

$$\phi_m = \phi_h = \left(1 + 5.2 \frac{z+z_0}{L}\right) . \tag{4.1.4}$$

It is hypothesised that buoyancy effects, e.g. in flow from a cold to a hot surface, are all accounted for by a change in L, and hence a change in the intensity of vertical mixing. A critical assumption is that the friction velocity, heat flux, velocity gradient, and temperature gradient are related by (4.1.1)-(4.1.4) not only in equilibrium flow above uniform surface conditions, but also

within the IBL developing downstream from the surface discontinuity.

No numerical results were obtained when the upstream flow was stable, because of problems with the finite-difference scheme. However satisfactory results were obtained for neutral and unstable upstream flow. Interesting predictions of the model were the following:

(i) Velocity profiles were relatively, but not completely, insensitive to a step change in surface temperature. Largest changes in the velocity occurred at the outer edge of the IBL, with velocity increasing when flow encountered an increase in surface temperature.

(ii) Treatment of heat as a passive property of the air gave important discrepancies (when compared with results with stability effects included) for downwind distances $x \geq 10^3 z_0$ (100m if z_0=1cm). At short downwind distances the errors were small, in agreement with the fact that at short fetch the IBL is confined to a shallow layer in which stability effects are expected to be unimportant. However, Taylor claims that stability effects become important as low as 25-50 cm and that in consequence simple heat-diffusion models will be inaccurate in cases where there is a significant change in the thermal conditions.

The model was used to simulate the experiment performed by Rider, Philip, and Bradley (1963), (see Section 5.1), and the predicted profiles compared reasonably well with experiment. Taylor attributes much of the inaccuracy

in the numerical results to lack of data for input to the model. One of his most definite conclusions is that 'the importance of changes in thermal stability in the leading-edge problem should not be underestimated.'

4.2 Weisman's Extension of the Model of Taylor

Taylor's numerical model has been extended by Weisman (1975) for application to the problem of the heat loss and evaporation from a body of water.

A vapour continuity equation was added to Taylor's set of equations,

$$u\frac{\partial q}{\partial x} + \omega\frac{\partial q}{\partial z} = -\frac{1}{\rho}\frac{\partial E}{\partial z}$$

where $$E = -\rho K_e \frac{\partial q}{\partial z} \quad .$$

The stability length was modified to include the buoyancy due to vapour stratification, becoming

$$L = \frac{-u_*^{\,3}}{k\frac{g}{T_0}\left(\frac{A}{\rho c_p} + 0.61\frac{E}{\rho}\right)} \quad .$$

The other modification chosen by Weisman was the use of a mixing-length that cannot increase without bound. This was found to be necessary to force the solution for a satisfactory distance downwind of the leading edge. He used the Blackadar mixing-length

$$l = \frac{k(z+z_0)}{1 + k(z+z_0)/\lambda}$$

which has the value λ in the limit as z tends to infinity, as opposed to the unbounded form $k(z+z_0)$ used by Taylor. Best results were obtained when λ represented a height corresponding to the depth of the surface layer.

Weisman concluded that the contribution of vapour buoyancy to sensible and latent heat fluxes and turbulent energy is significant, though less than the contribution of thermal buoyancy.

4.3 The Numerical Model of Rao, Wyngaard, and Cote

Rao, Wyngaard, and Cote (1974) presented a numerical model of airflow over a surface discontinuity. The model is restricted to steady two-dimensional flow. The equations used for the mean flow are the following, valid in all regions of the flow:

(i) The equation of continuity (2.1.5)

(ii) A horizontal momentum equation derived from (2.1.6) by neglecting horizontal pressure gradient and $\frac{\partial}{\partial x}\overline{u'^2}$ terms

$$u\frac{\partial u}{\partial x} + \omega\frac{\partial u}{\partial z} = \frac{\partial u_*^2}{\partial z}$$

(iii) A thermodynamic equation which neglects horizontal heat fluxes

$$u\frac{\partial \theta_p}{\partial x} + \omega\frac{\partial \theta_p}{\partial z} = -\frac{\partial}{\partial z}\overline{\omega'\theta_p'}$$

(iv) A vapour transfer equation

$$u\frac{\partial q}{\partial x} + \omega\frac{\partial q}{\partial z} = -\frac{\partial}{\partial z}\overline{\omega' q'}$$

where q is the mean specific humidity and θ_p is the mean potential temperature.

A higher-order closure technique is used, giving a set of 16 partial differential equations for the model. The lower boundary conditions are based on the equilibrium flux-profile relations given by Businger et al. (1971) and Wyngaard et al. (1971).

The model was applied to flow from an extensive smooth dry area onto grassy wet terrain, thus simulating the experiment performed by Rider, Philip, and Bradley (1963), (see Section 5.1). Excellent agreement with the experimental data was obtained. Important predictions of the model are:

(i) Most of the variation in the sensible and latent heat fluxes at the surface occurs within a few meters from the discontinuity.

(ii) The assumption of saturation at the surface overpredicts the modification occurring within the IBL.

(iii) The neglect of the effects of thermal stratification becomes increasingly important at longer fetches from the discontinuity. Only for very short (<5 m) fetches can heat be treated as a passive property of the airflow, because in this case the IBL is confined to the lowest layers of the atmosphere, where buoyancy effects are of lessened importance.

At longer fetches, the neglect of thermal stratification results in an error. However, because the

temperature modification at given fetch increases with decreasing height, at low levels the error is a small percentage of the actual modification. Close to the top of the IBL the error becomes comparable with the modification.

4.4 The Numerical Model of Novikova

Panchev, Donev, and Godev (1971) reported briefly the work of several Russian meteorologists who have studied problems of surface inhomogeneity.

Novikova (1969) gave an outline of a two-dimensional numerical model designed to study the effects of a discontinuity in surface temperature and moisture on arbitrarily stratified upstream flow. The equations used were the continuity equation, the momentum equation, the thermodynamic equation, a moisture transfer equation, and the turbulent energy equation. Fluxes were modelled using the mixing-length formulation of Laichtman.

Results were presented in graphical form, and are of little use in the current study. Novikova gave no comparison with experimental data.

CHAPTER 5

EXPERIMENTAL STUDIES OF TEMPERATURE-PROFILE MODIFICATION

5.1 The Experiment of Rider, Philip, and Bradley

Rider, Philip, and Bradley (1963) presented the first substantial set of data on the local advection of heat and moisture. Under conditions of steady insolation, these authors studied temperature-, wind-, and humidity- profile modification downwind of a discontinuity from tarmac to freely- evaporating, closely-mown grass. The change in roughness at the discontinuity was estimated to be

$$\frac{Z_0\ (\text{grass})}{Z_0\ (\text{tarmac})} = \frac{1 \cdot 4 \times 10^{-1}}{2 \times 10^{-3}} \sim 10^2$$

so that the change in roughness alone could be expected to produce important effects. However, the aim of the experiment was to study and compare with the Rider, Philip, and Bradley theory (see Section 3.3) the advection due to a discontinuity in moisture (and therefore temperature) conditions.

Forty-three acceptable observations were obtained, each of 10 minutes duration, and profile masts were placed at 0,1,4, and 16 m from the discontinuity. In general, the temperature profile showed strongly unstable lapse rates over the tarmac with gradual development of an advective

inversion over the grass.

The Rider, Philip, and Bradley model of local advection was used to calculate the temperature- and humidity-profile modification, the overall result of a large number of comparisons with observation being

$$\frac{[T(0,z) - T(x,z)]_{\text{calculated}}}{[T(0,z) - T(x,z)]_{\text{observed}}} = 2\cdot 3$$

$$\text{i.e.} \quad T(x,z)_{\text{observed}} < T(x,z)_{\text{calculated}}$$

and

$$\frac{[e(0,z) - e(x,z)]_{\text{calculated}}}{[e(0,z) - e(x,z)]_{\text{observed}}} = 1\cdot 06 \quad .$$

Predictions were most accurate in cases of large ΔT, Δe, i.e. for low heights and large fetches. The measured temperature differences were used in the predictions for humidity modification, which were more accurate than the temperature predictions. Rider, Philip, and Bradley consider the discrepancy in temperature prediction to be due to the change in roughness which is not considered in the model. It is estimated that the diffusivity over the grass would be greater than that over the tarmac by the ratio

$$\frac{K_{\text{grass}}}{K_{\text{tarmac}}} = 1\cdot 7$$

and therefore that stronger mixing over the grass would lead to lower temperatures in the IBL than the model predicts.

The increase in diffusivity through increased roughness would be partially countered by the increasing stability over the cooler grass, but the authors consider the effect of the roughness change on the diffusivity to be dominant in the air close to ground where stability effects are relatively weak.

Priestley, in a discussion of the Rider, Philip, and Bradley paper (Rider, Philip, and Bradley (1965)) does not agree that the poor temperature prediction is attributable solely to the roughness change. He points out that

$$u \propto Z^m \quad , \; m > 0$$

$$K \propto Z^{1-m}$$

is a poor approximation in unstable stratification, which occurred in almost all the experiments.

Rider, Philip, and Bradley concluded that their model should give accurate predictions of advective effects caused in situations not involving a change in roughness. Their experimental data has been used for comparison with the predictions of most of the numerical models of local advection.

5.2 The Observations of Dyer and Crawford

Dyer and Crawford (1965) reported data concerning airflow over dry unirrigated land onto a heavily-irrigated rye-grass field. Because the dry land received no rain all summer, while the rye- grass was supplied with 50 cm of water there was possibly a change in roughness at the boundary, but this is not stated. Measurements of temperature up to a height of 5 m were made as far downstream as 200 m from the leading edge.

Sensible-heat flux measurements at a height of 4 m and variable fetch indicated, on the assumption of zero heat flux at inversion height, that the heat flux at 4 m exceeded that at ground level by an amount which decreased with increasing fetch. In a two-dimensional problem,

$$A(0) - A(z) = c_p \int_0^z \rho u \frac{\partial T}{\partial x} \, dz$$

so that the non-constant heat flux indicates that horizontal homogeneity in temperature had not been attained over the irrigated land.

CHAPTER 6

INSTRUMENTATION, SITE, AND PROCEDURE OF THE ELLERSLIE EXPERIMENT

6.1 The Temperature Sensors

Wesely, Thurtell, and Tanner (1969) have described a fast-response unshielded resistance thermometer which is subject to very small radiation error. The thermometers used in this experiment differ from the above only in structural details, and their structure is shown in Fig. 6-1.

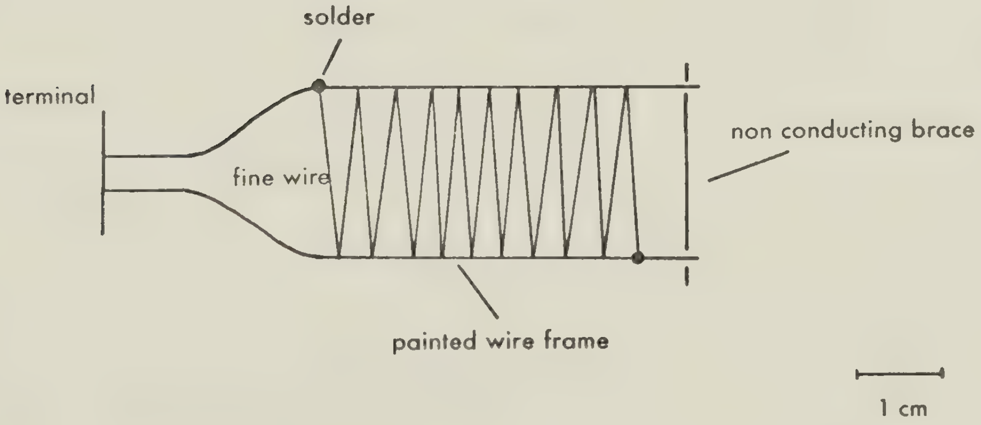

Figure 6-1. Structure of Temperature Sensors.

The frame was constructed of 1.6 mm diameter tinned copper wire, painted to form an insulated mount for the fine wire, leaving a small spot on each side for electrical contact. White paint was used in order that the equilibrium temperature of the wire would be as close as possible to that of the air. 8 to 10 cm of 5.6 μm diameter platinum-plated tungsten wire were then wound on to the frame, and the joints soldered. The resistance of the sensing element thus constructed was about 1500 ohms. The current supply circuitry was as shown in Fig. 6-2.

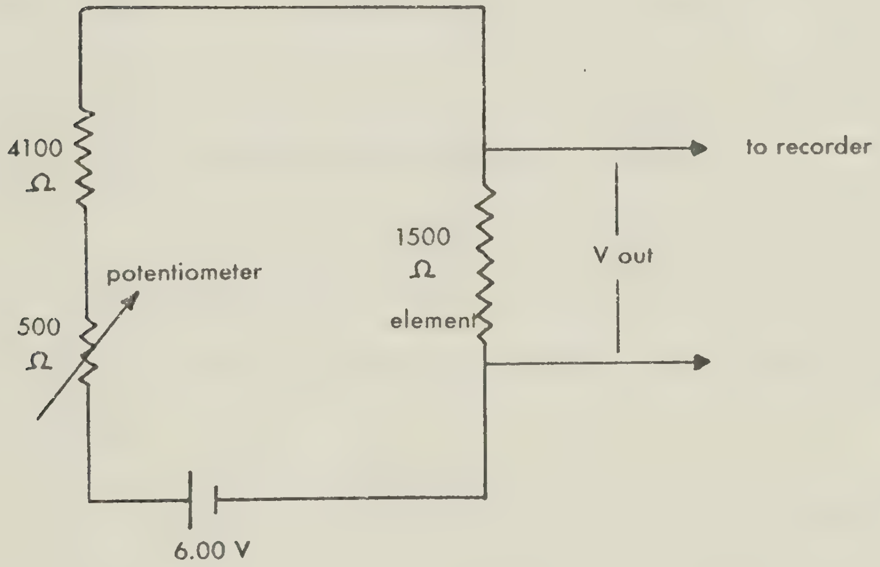

Figure 6-2. Sensor Power-Supply.

The current drawn by the element was of the order of 1 mA, and the voltage drop across it, V_{out}, approximately 1.5 V. A 5% change in the resistance of the fine wire would

give a change in V_{out} of approximately 4 mV.

Initially each sensing element had an individual 6 V power-supply, but problems were encountered with battery stability, and in operation all sensors were supplied by one regulated power-supply.

Wesely, Thurtell, and Tanner conservatively calculated that solar heating could cause an air-wire temperature difference of 0.15°C in still air, 0.09°C in a 5 $m\ s^{-1}$ wind. Provided all thermometers are equally exposed to radiation, solar radiation should not seriously affect the measurement of temperature differences. Testing prior to the Ellerslie experiment indicated that radiative heating would not be a significant problem.

6.2 The Temperature-Sensor Network

It was intended to set up a network of 12 resistance thermometers so that mean temperature differences within a spatial grid could be measured as accurately as possible.

The signal from each of the sensors was carried by shielded cable to a Honeywell 'electroniK 15' multichannel recorder. The recorder stepped through a cycle of twelve 5 second periods, during each of which the output voltages of a pair of sensors were differenced and amplified. The differencing pattern is shown in Fig. 6-3.

Just before the end of the 5-second period the amplified difference was recorded. A thirty-minute record

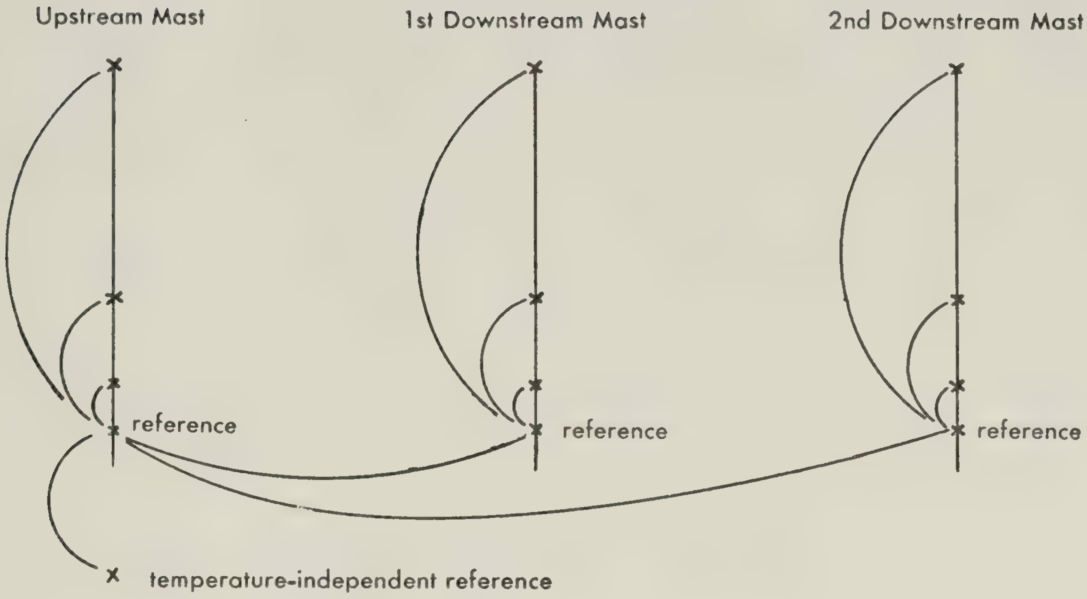

Figure 6-3. Pattern of Differences.

produced by the system contained, for each of the twelve temperature-sensor pairs, 30 differences each separated by one minute. Because the printing system was mechanically damped it is difficult to say whether the point plotted represented an average over the 5 seconds, or a shorter period. In the following discussion and throughout this report, each printed point will be regarded as an instantaneous value.

Consider an experiment during which N values are taken for each temperature difference. From the N values a sample mean can be established. On the assumption that the population of differences is approximately normal (which is shown to be the case in Section 7.1) and that sampling was random, a Student's t-test can be used to estimate the accuracy of the sample mean. Values of the standard

deviation of temperature difference, as measured in the Ellerslie experiment , varied according to the spacing of sensors and the stability, the range of values being 0.04 to 0.74°C. The t-test indicates that with a standard deviation of 0.3°C the chance of a 0.1°C or greater error in the mean temperature difference is 15% for N=20, but approximately 0% for N=120. The chance of an error of 0.05°C or greater is 50% for N=20, 7% for n=120. The t-test indicates that if the desired accuracy in the temperature differences is better than 0.05°C then the value of N should be somewhat greater than 20.

A simple criterion governing choice of the sampling rate for mean profile measurements has been given by Kaimal (1975) :

$$N \gtrsim \left(\frac{\sigma(x)}{\Delta x}\right)^2$$

where $\sigma(x)$ is the standard deviation of x, and Δx is the desired accuracy. Unfortunately this criterion was not considered prior to execution of the Ellerslie experiment, in which the combination of the need to use a single recorder for many differences, the need to cover many positions with sensors, and the limitation on sampling time imposed by the need for stationary conditions restricted values of N to at most 40 (sunny conditions) and more often 20, values which were erroneously thought to be satisfactory. In some cases N was further reduced by the rejection of data to ensure that averaging was performed

over stationary conditions. Confidence in the mean temperature differences could have been improved by obtaining a greater number of data points in each experiment.

CALIBRATION

Temperatures for the calibration procedure were measured using "ZEAL" mercury thermometers certified by the Atmospheric Environment Service and accurate to within ±0.1°F.

Calibration began by placing all 12 thermometers in a draughtless environment on a frame enclosed within a thick polystyrene box, the aim being to hold all sensors at an identical temperature. It was established that about 20 minutes after being closed, the temperature within the empty polystyrene box would become uniform to within the accuracy of the thermometers available. However, with the frame and sensors in the box, great care had to be taken that there was in fact temperature uniformity. It was found that air contained in plastic film containers, which formed the weather protection for sensor wiring, would equillibrate so slowly as to give an anomalous local temperature up to half an hour after closing the box. Holes drilled in the plastic cured this.

When uniform temperature had been established, and thus all temperature differences were zero, the recorded differences were adjusted to chosen zero positions using the

potentiometers seen in Fig. 6-2.

Calibration required measurement of the recorded shift away from zero position when a pair of sensors was held at different (known) temperatures. To perform this measurement , use was made of a second polystyrene box which was ventilated with a flow of cold air. Even with the airflow the temperature in this box was found to be uniform to within the limits of accuracy of the calibrating thermometers. One by one each sensor was separated from the other 11 and the response (recorder divisions / °C) was measured. The tests were repeated as often as time allowed in order to try to arrive at an accurate mean calibration. Initially it was not assumed that the calibration factor for all sensor-pair differences would be the same, but after many trials, the variation between repeated trials on any one pair was similar to that between pairs, so that a single number was eventually chosen for all pairs.

BEHAVIOUR OF THE MEAN TEMPERATURE SENSOR NETWORK

The resulting system behaved unsatisfactorily in only one respect. Trouble was experienced intermittently, with no channels being completely exempt, when the recorded number for zero temperature difference would jump or drift rapidly ; this phenomenon is hereafter referred to as a "zero shift". This meant that the signal voltages arriving at the recorder were changing by some mechanism other than change in the resistance of the temperature sensors, because

any problem arising in the recorder would be expected to have similar effects on all channels (this was not observed to be the case). It was established that the zero shifts were not caused by wetness of the various connections, but nonetheless equipment was stored inside to avoid wetting connections. With no explanation for this inconvenient behaviour being found, it was decided that the problem probably arose from changes in the resistance of some of the many joints and terminals in the system. Because the temperature sensor output voltages being measured were very small, $\sim$5 mV, small extraneous resistance changes would have a large effect.

The problem was dealt with by frequent testing of the recorder zero positions, usually both before and after each experiment. This necessitated movement of all the masts and cables, and transfer of sensors into a small volume in which mean temperature differences were assumed to be zero. Although this was very inconvenient, and may even have aggravated the problem, it was necessary in order that the data obtained should not be misinterpreted. In fact, interpretation of the data was in many cases difficult and in several cases impossible, because of the zero shifts.

6.3 The Sonic Anemometer-Thermometer

During each experimental run, vertical velocity and temperature at 280 cm were sampled at 50 or 100 Hz by a sonic anemometer-thermometer, filtered at 20 Hz, digitized, and recorded on magnetic tape. This data provided a means of calculating the heat flux, of interest in its own right, and also as an indicator of how steady the meteorological conditions were for the experiment.

The sonic anemometer-thermometer was of the type described by Kaimal and Businger (1966).

Kaimal and Businger show that

$$\phi_2' - K\phi_1' = -\frac{4\pi K f_1 \omega' d}{\bar{c}^2}$$

$$\phi_2' + K\phi_1' = \frac{2\pi K f_1 T' d}{\bar{c}\bar{T}}$$

where 1 indicates properties of the upward pulse and 2 indicates properties of the downward pulse; f is frequency, ϕ' change in phase, w′ change in vertical velocity, T′ change in temperature, $\bar{c}$ the mean speed of sound, and d the separation of the microphone-receiver pairs. The ratio of the frequencies is given by $K=f_2/f_1$.

Recording is performed so that

$$\phi_2' - K\phi_1' = \alpha n_\omega'$$

$$\phi_2' + K\phi_1' = \beta n_T'$$

where n_ω' is the change in n_ω, the number recorded representing vertical windspeed, and n_T' is the change in n_T, the number recorded representing temperature.

The sonic-anemometer record was used to calculate the sensible- heat flux, the covariance between fluctuations in vertical windspeed and fluctuations in temperature:

$$A = \rho c_p \left(\frac{-\bar{c}^2}{4\pi K f_1 d} \alpha \right) \left(\frac{\bar{c}\,\bar{T}}{2\pi K f_1 d} \beta \right) \overline{n'_\omega n'_T} = \text{constant} \times \overline{n'_\omega n'_T} \;.$$

Calibration performed several times throughout the series of experiments determined α and β .

6.4 Shear-Stress Meter and Humidiometer

The shear-stress meter consisted of three polystyrene propellor anemometers mounted accurately on a mast so as to be mutually perpendicular. The output of the anemometers was filtered, digitized, and recorded on magnetic tape.

The anemometers had a response time of 0.3 s, a threshhold of 0.3 m s^{-1}, and a linear response to windspeeds from 1.2 to 22 m s^{-1}. Low magnitude and frequent reversals of the vertical wind lead to a calibration problem for the vertical anemometer. Berntsen (1971) considered this problem , and found that the non-linear propellor response has a more noticeable effect on heat-flux cospectra than on the spectra of the vertical wind. On average he found

$$\frac{(\text{standard deviation of } \omega)_{\text{sonic}}}{(\text{standard deviation of } \omega)_{\text{shear stress meter}}} = 1\cdot 3 \qquad ,$$

$$\frac{(\text{heat flux})_{\text{sonic}}}{(\text{heat flux})_{\text{shear stress meter + fine wire}}} = 2 \quad .$$

The response of the propellors to the horizontal wind should be satisfactory except for very high frequencies.

In view of the findings of Berntsen, quoted values of $u_* = \left(-\overline{w' V'}\right)^{1/2}$ are twice the measured values.

The flux of latent heat was measured using an Electromagnetic Research Corporation Lyman Alpha humidiometer. This was calibrated after the Ellerslie experiment was performed, prior to data analysis. Latent heat fluxes quoted in Chapter 7 were obtained by calculating the covariance between signals from the sonic anemometer and the humidiometer, which were mounted at z=280 cm and separated horizontally by 40 cm. The large separation between humidiometer and anemometer probably lead to an underestimate of the latent heat flux, but this is not a critical point because the flux has not been used in any calculations.

6.5 Retrieval of Data from Magnetic Tape

The magnetic tape recording system could record a maximum of 8 channels, of which 7 could be filtered at optional frequency before digitizing. The sampling rate was most often 50 or 100 Hz on each channel.

The data were retrieved by a computer program which would calculate the means, standard deviations, and chosen covariances over any time period chosen. Covariances were calculated using the formula

$$\overline{x'y'} = \overline{xy} - \overline{x}\,\overline{y}$$

where a prime denotes a fluctuating quantity.

Shear stress, the covariance between horizontal windspeed in the mean direction and the vertical windspeed, was calculated using the formula

$$\overline{V'w'} = \overline{uw}\sin\theta + \overline{vw}\cos\theta - \overline{V}\,\overline{w}.$$

where $\tan\theta = \bar{u}/\bar{v}$, V is the horizontal windspeed in the mean direction, and θ is the direction of the mean wind.

Use of double precision ensured that variables did not overflow even when sums of products for covariances were accumulated for one hour of data. The program was tested on artificial data.

6.6 Experimental Site

The experiment was performed during late July and August of 1975 in a fairly level field at the University Farm, Ellerslie, Alberta. Fig. 6-4 shows a plan of the field site.

It can be seen that the extent of horizontal uniformity upstream of the irrigated plot was at most about 100 m. Had wind direction during August been predominantly NW, as is usual, the site would have allowed the considerably longer uniform upwind distance planned for.

The grass was mown before experimentation began, in late July , so that roughness was uniform within the boundaries shown in Fig. 6-4, and of magnitude approximately 1 to 2 cm.

Portable aluminum irrigation piping was available in 6.1 m lengths, and water was supplied to the system from a water truck. Use of the portable system allowed the water to be placed downwind of the 6 m tower for a range of wind directions of about 90°. Six lengths of piping plus a perforated plastic hose forming the leading edge gave an irrigated area of about 20 m by 20 m, and the water truck generally placed about 1200 gallons of water on this area prior to an experiment.

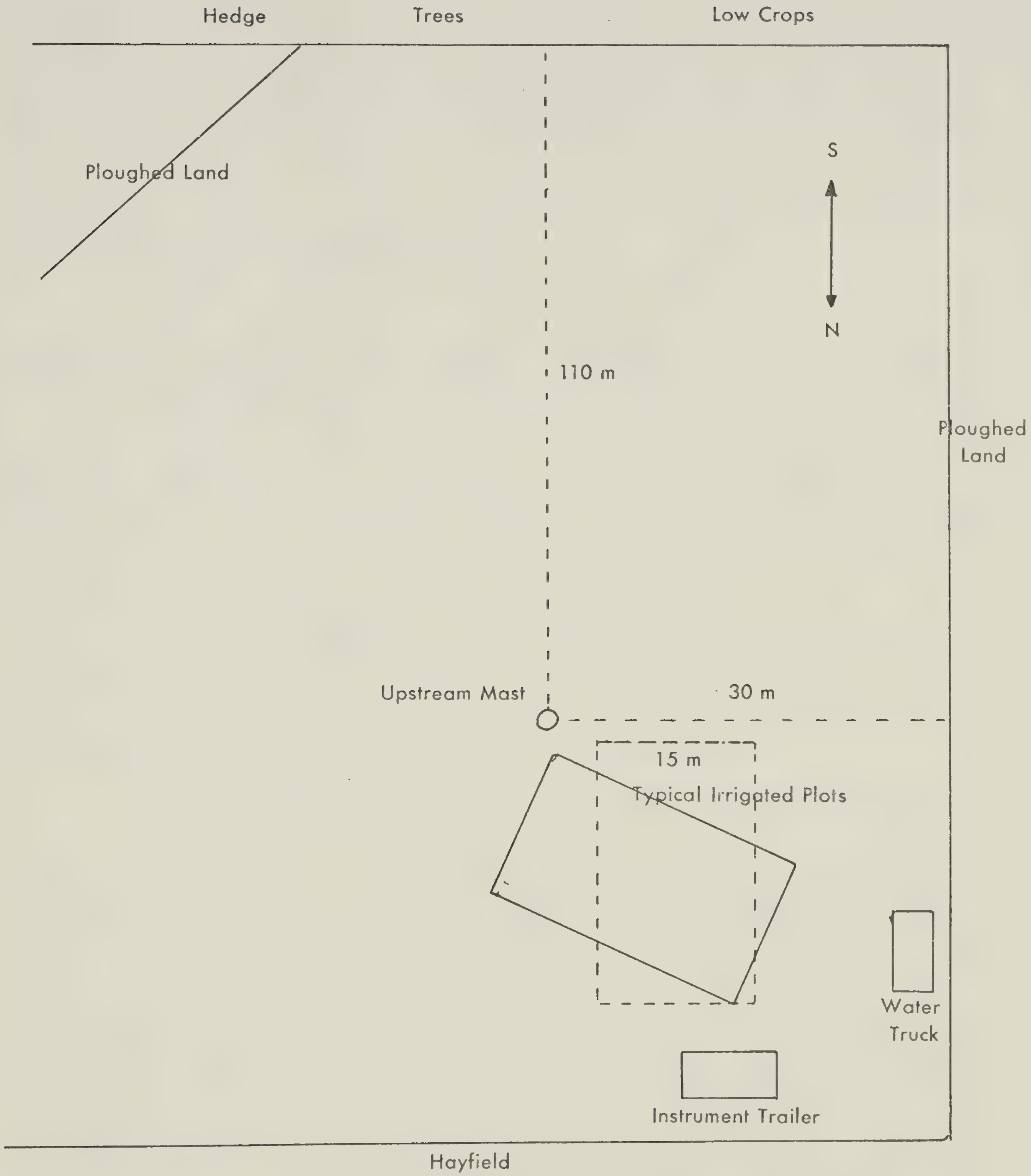

Figure 6-4. The Experimental Site.

6.7 Instrument Layout

The instruments were arranged to provide as much information as possible about the spatial changes in the air as it passed over the surface discontinuity and downwind over the irrigated plot. The fast-response instruments were placed at a height of 280 cm on the 6 m tower to monitor conditions in the oncoming flow.

During several of the experiments, one of the net radiometers available was placed over the wet grass, while in all experiments the net radiation over the dry grass was recorded. During each experiment two dewpoint sensors were placed on a small portable mast on the irrigated plot, and two were mounted upstream on the 6 m tower.

The 6 m upstream tower held a set of propellor anemometers at heights of 30, 54, 114 ,233, and 470 cm, and temperature sensors at 30, 60, 120, and 240 cm.

The downstream masts were necessarily portable, because of variable wind direction. Two light 3 m towers were used, each holding four temperature sensors and three anemometers. The experiment was run for a period considered the minimum sufficient to give meaningful averages under the prevailing conditions (20 minutes if overcast, 40 minutes if sunny[1]) with the downstream masts at 5 and 15 m from the discontinuity. If the grass was still wet the masts were

---

[1] As has been stated in Section 6.2, these averaging times did not yield a satisfactory number of data points in some experiments.

quickly moved to 10 and 20 m and the experiment continued.

The guidelines provided by Rider, Philip, and Bradley (1963) were used to match the anemometer and temperature-sensor heights to the expected height of the IBL. Heights used were usually:

FETCH (m)	HEIGHTS OF TEMPERATURE SENSORS (cm)			
0	30	60	120	240
5	20	40	80	160
10	20	40	80	160
15	30	60	120	240
20	30	60	120	240

Figures 6-5 and 6-6 show the layout of the instruments.

6.8 Experimental Procedure

In order that a good moisture discontinuity be obtained, the experiment could only be performed if there had been negligible rain for at least the previous 24 hours. If this condition was satisfied, and a favourable wind direction was forecast, the instruments were set up and tested early in the day. When conditions became satisfactory the irrigation piping was laid down and watering began. It took about half an hour to discharge the 1200 gallons, during which time the temperature sensors were all placed together and the recorder zeros established. The piping was then quickly removed (1/2 minute) and the

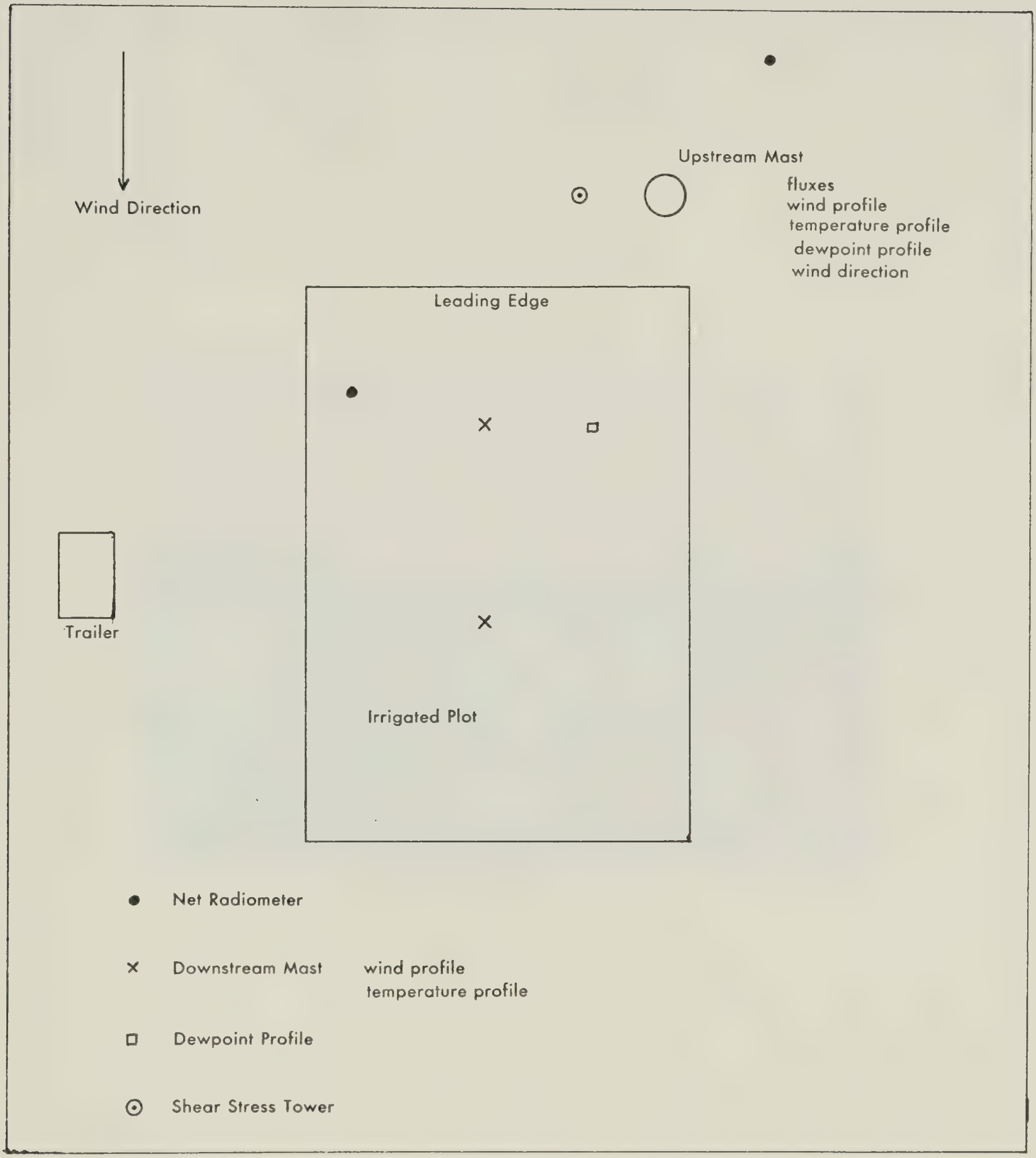

Figure 6-5. Instrument Layout.

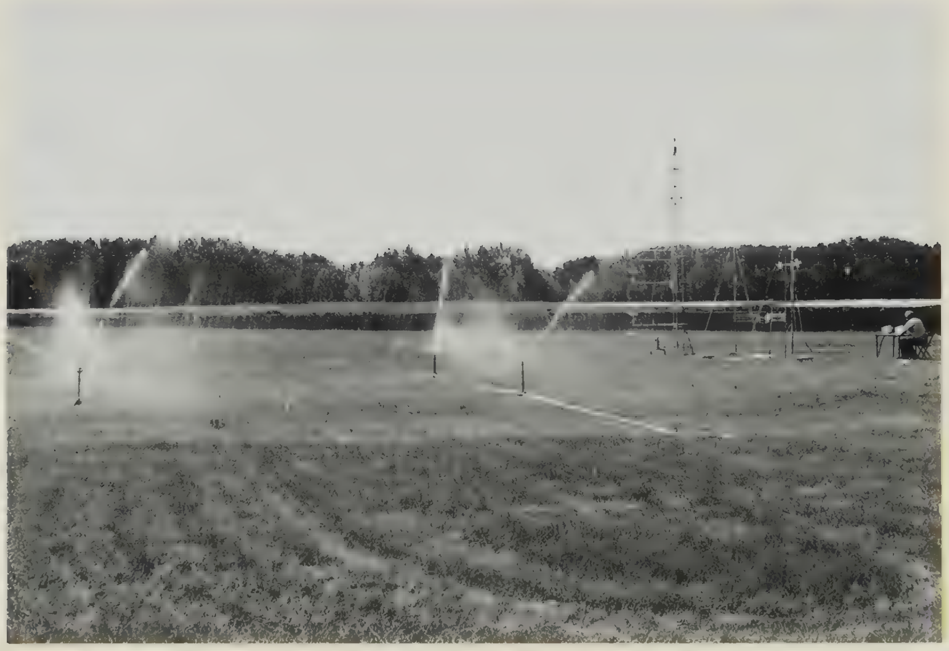

Figure 6-6. Photograph showing Layout. (Temperature sensors grouped to perform zeroing).

downstream masts placed on the plot (1 minute). Averaging then began, and was continued for 20 to 40 minutes after which time the downstream masts were shifted and the performance repeated. The temperature sensors were then re-zeroed, and if conditions were still satisfactory re-irrigation began for another experiment.

Throughout each day, wind profiles were measured continuously on the 6 m tower. This enabled the construction of a record of the upstream wind profile, and interpolations could be made for any desired time interval provided wind behaviour was reasonably steady.

With the large number of instruments involved in the experiment, and the necessity of moving masts and cables, running the experiment required four people to be reasonably familiar with the procedure.

CHAPTER 7

TEMPERATURE-PROFILE MODIFICATION

7.1 Temperature-Profile Modification Data

Six experiments, ranging in length from 12 to 39 minutes and including a wide range of atmospheric stability conditions have been selected for detailed study. The remaining experiments were rejected because of unsuitable wind direction, large time changes in atmospheric stability, or zero shifts in the mean- temperature network (see Section 6.3).

Table 7-1 lists, for each experiment, the wind, cloud, energy balance, temperature, and stability conditions in the upstream flow.

Table 7-2 gives the upstream and downstream mean temperature profiles observed in each experiment. Temperature differences between the masts are also given, but it should be noted that not all these differences were taken between sensors at equal heights, so that these differences were not all horizontal. Possible sources of inaccuracy in the temperature-difference data are, in order of importance:

(i) Zero shifts (see Section 6.2) which lead to systematic errors which were in many cases hard to

Experiment Number	1	2	3	4	5	6
Date	07AUG75	14AUG75	26AUG75	26AUG75	26AUG75	26AUG75
Time (MDT)	1409-1434	1322-1401	1623-1635	1802-1818	1829-1849	1852-1912
Mean Windspeed at 270 cm (m s^{-1})	3.0	3.7	3.9	3.6	3.5	3.0
Wind Direction and Range (°)	140±40	245±45	110±20	120±20	110±20	105±20
Effective Fetches of Downstream Masts (m)	10,20	6,15	11,20	10,20	5	11
Friction Velocity (m s^{-1})	.26	.55	.60	.46	.49	.38
Cloud Conditions	$\frac{10}{10}$, TCU,CB	clear	$\frac{7}{10}$CU,$\frac{1}{10}$CI	$\frac{3}{10}$TCU, $\frac{4}{10}$AC	$\frac{3}{10}$TCU, $\frac{4}{10}$AC	$\frac{2}{10}$TCU, $\frac{3}{10}$AC
Net Radiation (mW cm^{-2})	+8	+49	+15	+15	+2	+3
Sensible Heat Flux (mW cm^{-2})	+1	+8	n/a	+11	-3	-2
Latent Heat Flux (mW cm^{-2})	+11	+3	+3	+2	n/a	+1
Gradient Richardson Number at 85 cm	+0.02	-1.2	-0.03	-0.1	+0.2	+0.1
Local Ambient Temperature (°C)	21	21	17	17	16	16

Table 7-1. Experimental Conditions.

EXPERIMENT NUMBER 1

(a) Vertical Differences

		Fetch (cm)		
		0	1000	2000
	240	+0.73(.16)	+1.35(.26)	+1.22(.26)
	160			
	120	+0.42(.16)	+0.80(.20)	n/a
Height	80			
(cm)	60	+0.16(.10)	+0.51(.16)	+0.53(.33)
	40			
	30	T_0	T_{10}	T_{20}
	20			

(b) Differences between masts

$T(1000,30)-T(0,30) = -0.29(.30)$

$T(2000,30)-T(0,30) = -0.71(.33)$

Table 7-2. Mean Temperature Differences (°C) and Sample Standard Deviations.

EXPERIMENT NUMBER 2

(a) Vertical Differences

Height (cm)	Fetch (cm)		
	0	600	1500
240	T_0		
160		T_6	T_{15}
120	+0.48 (.23)		
80		+0.63 (.28)	+0.44 (.22)
60	+1.11 (.48)		
40		+1.01 (.48)	+0.70 (.41)
30	+2.41 (.36)		
20		+1.42 (.44)	+1.05 (.53)

(b) Differences Between Masts

$T(600,160) - T(0,240) = +0.49\ (.61)$

$T(1500,160) - T(0,240) = +0.44\ (.74)$

Table 7-2 (continued). Mean Temperature Differences (°C) and Sample Standard Deviations.

EXPERIMENT NUMBER 3

(a) Vertical Differences

		Fetch (cm)		
		0	1100	2000
	240	T_0		T_{20}
	160		T_{11}	
	120	+0.08(.04)		+0.04(.06)
Height	80		-0.10(.09)	
(cm)	60	+0.10(.07)		-0.18(.14)
	40		-0.28(.09)	
	30	+0.27(.19)		-0.40(.16)
	20		-0.52(.19)	

(b) Differences Between Masts

T(1100,160)-T(0,240)= -0.06(.08)

T(2000,240)-T(0,240)= -0.03(.05)

Table 7-2 (continued). Mean Temperature Differences (°C) and Sample Standard Deviations.

EXPERIMENT NUMBER 4

(a) Vertical Differences

		Fetch (cm)		
		0	1000	2000
	240	T_0		T_{20}
	160		T_{10}	
	120	+0.10(.08)		0.00(.07)
Height	80		-0.08(.05)	
(cm)	60	+0.14(.13)		-0.16(.11)
	40		-0.11(.12)	
	30	+0.27(.33)		-0.28(.18)
	20		-0.41(.17)	

(b) Differences Between Masts

$T(1000,160)-T(0,240) = +0.06(.15)$

$T(2000,240)-T(0,240) = -0.03(.09)$

Table 7-2 (continued). Mean Temperature Differences (°C) and Sample Standard Deviations.

EXPERIMENT NUMBER 5

(a) Vertical Differences

		Fetch (cm)	
		0	500
	240	T_0	
	160		T_5
	120	-0.26(.06)	
Height	80		-0.31(.06)
(cm)	60	-0.38(.10)	
	40		-0.52(.10)
	30	-0.49(.13)	
	20		-0.80(.14)

(b) Differences Between Masts

$T(500,160)-T(0,240) = -0.22(.16)$

Table 7-2 (continued). Mean Temperature Differences (°C) and Sample Standard Deviations.

EXPERIMENT NUMBER 6

(a) Vertical Differences

		Fetch (cm)	
		0	1100
	240	T_o	
	160		T_{11}
	120	-0.26(.06)	
Height	80		-0.31(.08)
(cm)	60	-0.31(.09)	
	40		-0.44(.08)
	30	-0.39(.16)	
	20		-0.68(.13)

(b) Differences Between Masts

T(1100,160)-T(0,240) = -0.16(.12)

Table 7-2 (continued). Mean Temperature Differences (°C) and Sample Standard Deviations.

detect, and could not be included in the uncertainty analysis.

(ii) An insufficient number of sample points in the shorter experiments, leading to wide confidence limits.

The between-mast differences in experiments 1 and 2 have not been used in all sections of the analysis, because they imply that warming occurred over the cool surface at several levels. A plausible explanation of this would be the occurrence of zero shifts in the sensor system, but it cannot be proven that such systematic error was responsible for the warming indicated. Such warming in experiments 1 and 2 would be inconsistent with the cooling over the wet surface which is expected and was observed in experiments 3 to 6.

The cooling observed over the wet surface in experiments 3 to 6 is shown in Table 7-3, with an average cooling being given for each height on each mast. The contributions to each average from the respective experiments were weighted according to the length of the experiment. The uncertainties given are at the 95% confidence level, and were calculated by:

(i) Calculating the standard deviation of the enlarged sample for each height

(ii) Using the student's t-test with the above standard deviation.

Formally, the student's t-test may only be used to obtain

		EXPERIMENT NUMBER				
		3	4	5	6	AVERAGE
1st Mast	120 cm	-0.18 (.13)	-0.08 (.18)	-0.07 (.18)	-0.08 (.16)	-0.09±0.05
	60 cm	-0.32 (.14)	-0.17 (.22)	-0.24 (.20)	-0.21 (.17)	-0.23±0.05
	30 cm	-0.71 (.25)	-0.37 (.39)	-0.35 (.24)	-0.27 (.22)	-0.39±0.08
2nd Mast	240 cm	-0.03 (.05)	-0.03 (.09)	n/a	n/a	-0.03±0.02
	120 cm	-0.07 (.09)	-0.13 (.14)	0.00 (.19)	+0.03 (.15)	-0.03±0.04
	60 cm	-0.31 (.16)	-0.33 (.19)	-0.11 (.25)	-0.18 (.17)	-0.22±0.05
	30 cm	-0.70 (.25)	-0.58 (.39)	-0.26 (.25)	-0.22 (.24)	-0.40±0.09

Table 7-3. Cooling over the Wet Surface (°C) and Sample Standard Deviation.

confidence intervals for the sample mean when the sample is randomly selected from a normal distribution. In practise, however, it has been found that the confidence intervals defined by the t distribution are satisfactory even if the distribution of the variable of interest is only close to normal.

Temperature differences were sampled randomly in the Ellerslie experiment. In order to test the normality of the distribution of the temperature differences a large sample of 650 differences covering both unstable and stable conditions on the 26th of August was chosen. Fig. 7-1 shows the distribution of these differences on probability paper. It is evident that the distribution is close to normal, hence use of the t-test to derive confidence intervals for the temperature-difference data is justified. It has been noted in Section 6.2 that confidence in the mean temperature differences could have been improved by obtaining a greater number of sample points in each experiment.

It can be seen from Table 7-3 that the amount of cooling does not differ significantly between the two masts at the 95% confidence level. If the cooling on both masts is combined to form a grand average, the resulting cooling is:

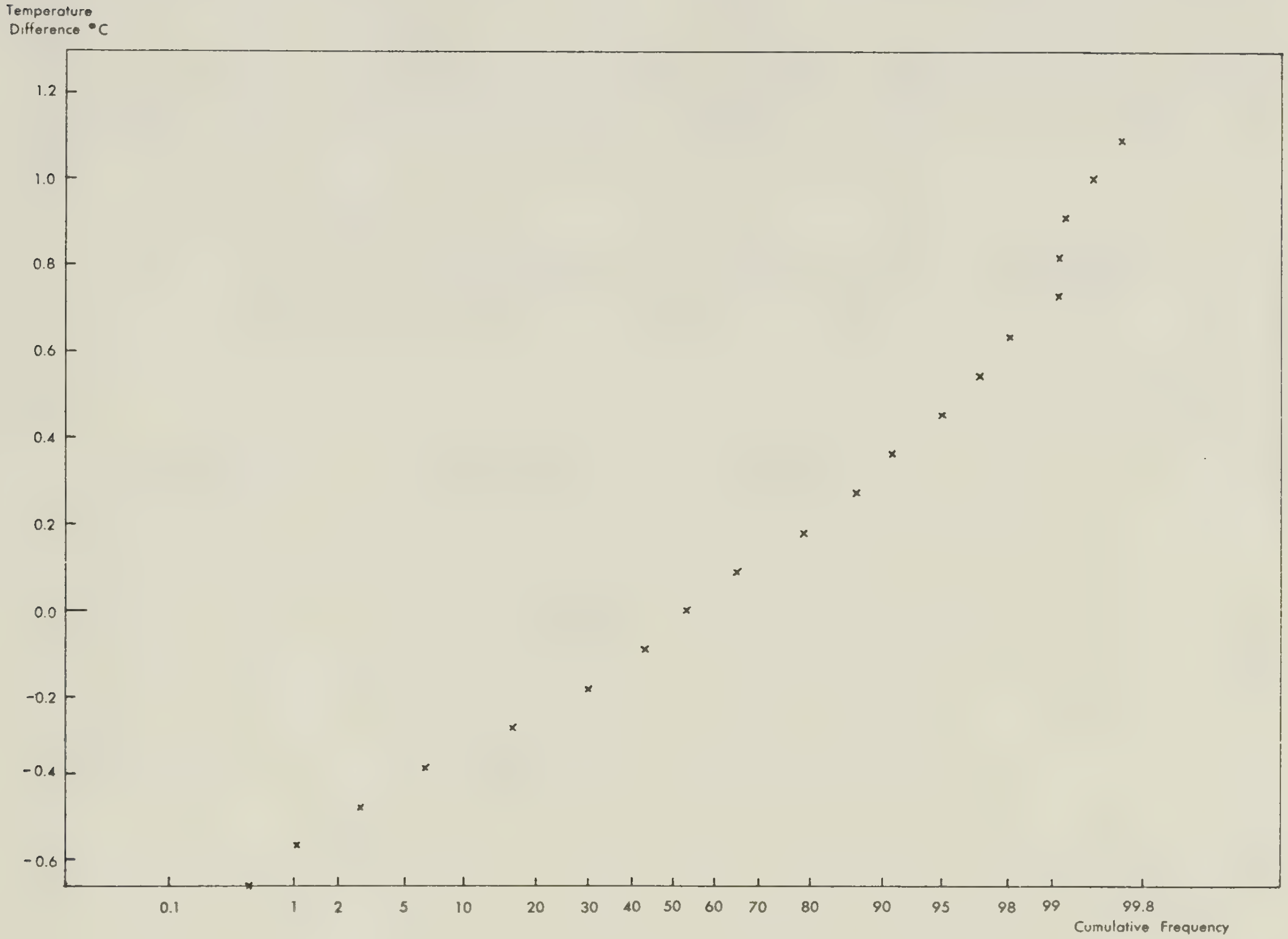

Figure 7-1. Distribution of Temperature Differences.

240 cm	-0.03±0.03 °C
120 cm	-0.06±0.03
60 cm	-0.23±0.03
30 cm	-0.40±0.06 .

The uncertainties above are again at the 95% confidence level, and are calculated by the method given earlier. Fig. 7-2 shows this overall average cooling as well as that on the individual masts.

If the downstream cooling data is broken into stable and unstable cases the results obtained are:

Height (cm)	Unstable	Stable
240	-0.03±0.03 °C	n/a
120	-0.11±0.04	-0.03±0.04
60	-0.28±0.03	-0.19±0.06
30	-0.57±0.10	-0.28±0.08

These values are plotted in Fig. 7-3. The cooling at 30 cm is significantly stronger under unstable conditions than under stable conditions, while at 60 cm and 120 cm the difference is not significant at the 95% confidence level. Stronger cooling under unstable conditions is expected because in such cases the magnitude of the temperature step at the leading edge should be larger than under stable conditions.

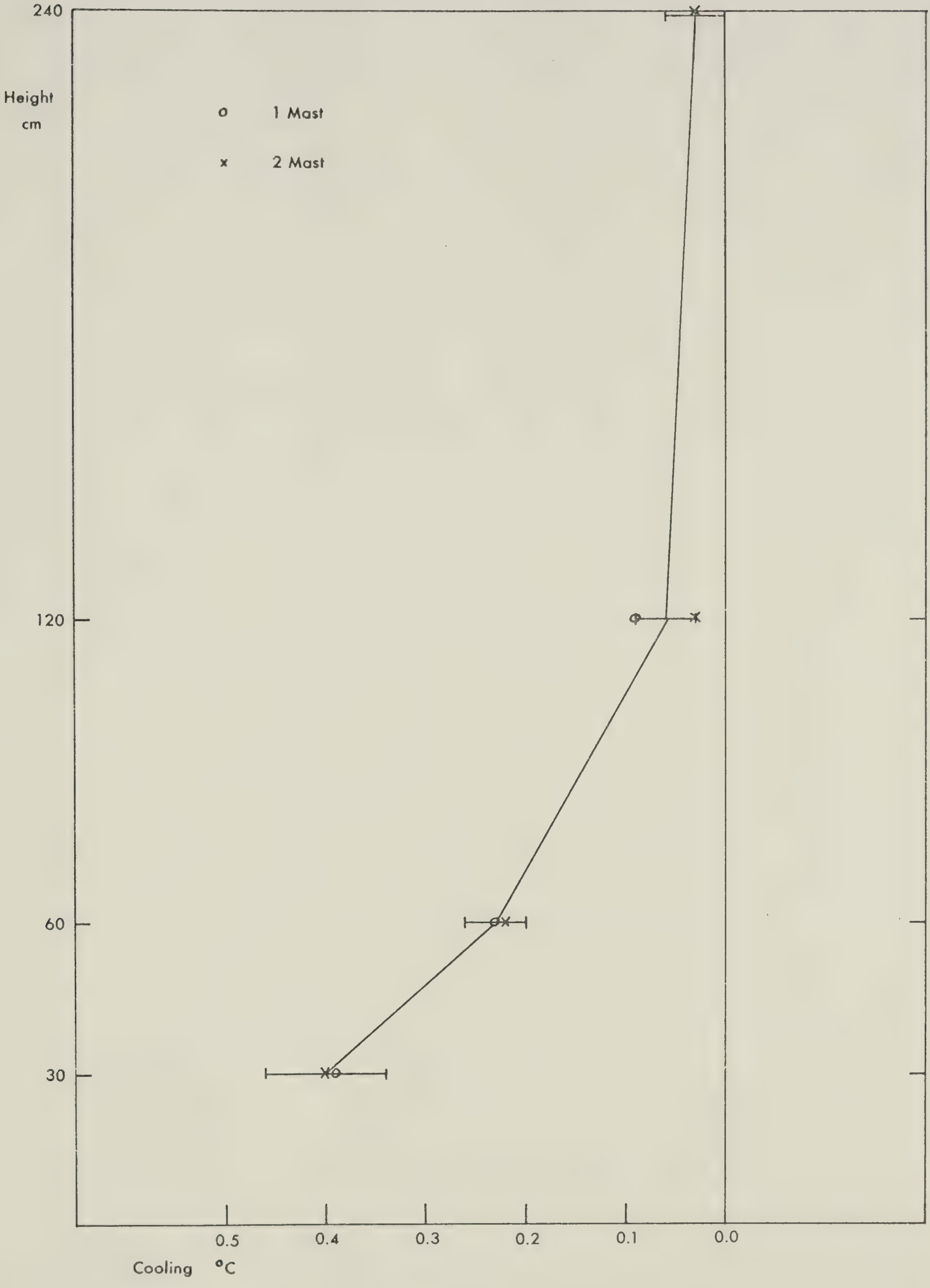

Figure 7-2. Cooling over the Wet Surface.

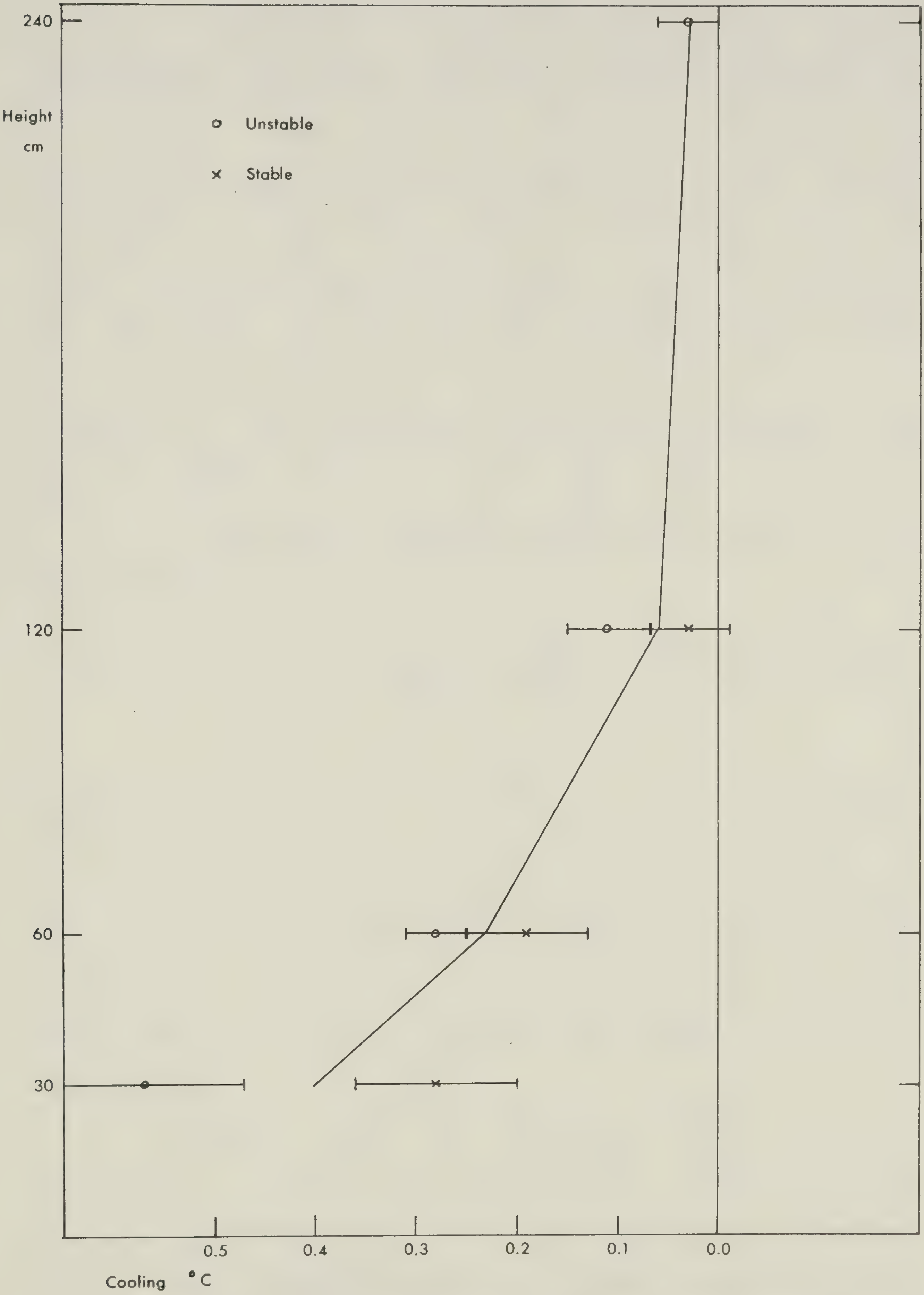

Figure 7-3. Cooling over the Wet Surface under Stable and Unstable Stratification.

So far in the analysis of experimental results discussion has been concerned with the cooling of the air as it passes onto the wet surface, expressed as upstream-downstream temperature changes at each height considered. However the effect of the step change in surface temperature on the airflow may also be considered from the point of view of the changes in the vertical temperature gradient. Such an approach does not require knowledge of the between-mast temperature differences, and thus experiments 1 and 2 may be included in the analysis.

A temperature-gradient stabilisation parameter can be defined as follows:

$$S(x, \sqrt{z_1 z_2}) = \left[\frac{T(x,z_2) - T(x,z_1)}{z_2 - z_1}\right] - \left[\frac{T(0,z_2) - T(0,z_1)}{z_2 - z_1}\right].$$

It is expected that S will be positive regardless of the upstream stratification, and that it will decrease rapidly with height because a step decrease in surface temperature will have greatest effect on the temperature gradient close to the ground. Greatest values of S are likely to occur under conditions which maximise the change in surface temperature.

Table 7-4 gives the values of S(x,z) for all experiments. In all but three cases, values of S are positive, the exceptions being only very small negative values. The expected decrease of S with increasing height is observed, and its maximum values occur in experiment 2,

		Experiment Number					
Layer	Mast	1	2	3	4	5	6
240/120	1st	.20±0.17					
	2nd	-0.03±0.13		0.03±0.05	0.08±0.09		
160/80	1st	-0.01±0.23	-0.06±0.15	0.18±0.07	0.13±0.10	0.25±0.05	0.29±0.06
	2nd	0.14±0.23	0.18±0.14	0.19±0.07	0.18±0.12		
120/60	1st	0.05±0.23	0.27±0.21	0.26±0.10	0.15±0.12	0.28±0.06	0.22±0.06
	2nd	0.25±0.23	0.52±0.21	0.40±0.12	0.34±0.13		
80/40	1st	0.58±0.21	1.10±0.25	0.68±0.12	0.33±0.17	0.23±0.09	0.15±0.10
	2nd	0.68±0.19	1.40±0.23	0.81±0.14	0.63±0.18		
60/30	1st	1.12±0.20	2.96±0.26	1.30±0.17	0.66±0.22	0.36±0.12	0.20±0.16
	2nd	1.23±0.23	3.33±0.27	1.30±0.19	0.83±0.23		

Table 7-4. Stabilisation of the Temperature Gradient over the Cool Surface (°K m^{-1}).

during which the net radiation, and therefore the step in surface temperature, was larger than in any other experiment.

It is also evident that the stabilisation of the temperature gradient relative to the upstream stratification increases with increasing fetch over the cool surface, but by an amount which is not significant at the 95% confidence level. Although it is to be expected that the downstream stratification should be increasingly stabilised with increasing fetch until a new equilibrium profile is established over the cool surface, the data indicates no significant effect, and that averaging over both masts will not result in a loss of information.

Fig. 7-4 shows the values of S plotted against height for each experiment. The mean value at each height is also shown. The error bars shown on the mean curve give the uncertainties in the means at the 95% confidence level, calculated using the t-test. The mean values are:

170 cm	0.07±0.07 °K m^{-1}
113	0.15±0.06
85	0.28±0.11
57	0.66±0.18
42	1.33±0.32

Because the temperature profiles were measured at varying fetches, the mean curve applies at the mean fetch,

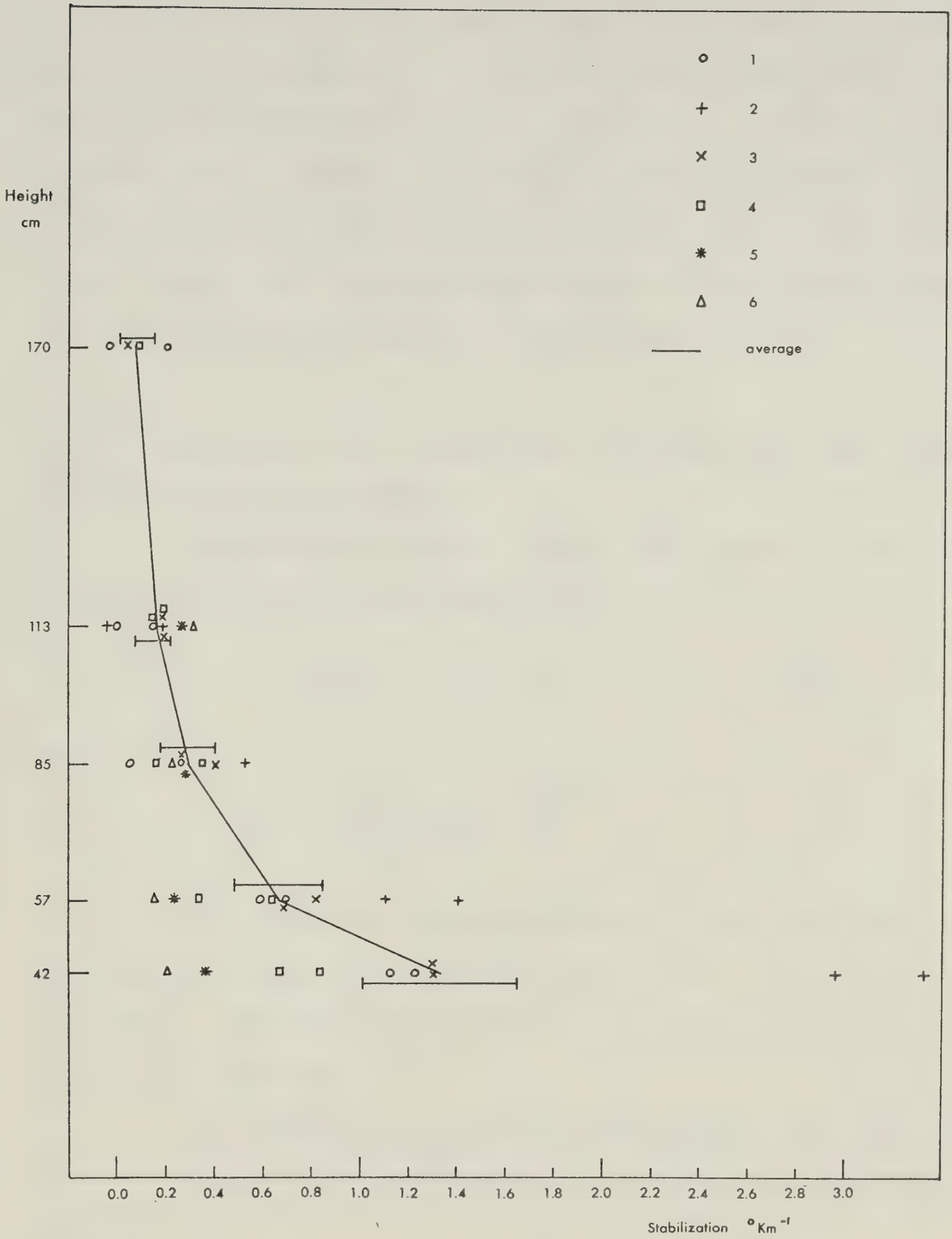

Figure 7-4. Stabilisation of the Temperature Gradient over the Cool Surface.

which was 13 m. The mean curve thus gives the average stabilisation expected at 13 m fetch over an irrigated grass surface of roughness 1 to 2 cm , with the averaging being applied over several experiments covering unstable and stable stratification. In Section 7-3 this experimental mean curve will be compared with that given by the Rider, Philip, and Bradley model of local advection.

7.2 Calculation of Parameters Required by the Rider, Philip, and Bradley Model

The model of Rider, Philip, and Bradley (1963) for temperature-profile modification is

$$T(x,z) - T(0,z) = \Delta T_0 \left[1 - I\left(\eta_T , - \frac{1+m}{1+2m} \right) \right]$$

where

$$\eta_T = \frac{u_1 \, z_1^{\,1-2m}}{K_1 \, (1+2m)^2} \; \frac{z^{1+2m}}{x} \quad .$$

To compare the predictions of the model with the experimental data the parameters m, u_1/K_1, and ΔT_0 are required. The reference height z_1 was chosen as 30 cm, and T(0,z) was measured.

The power law parameter m was chosen by plotting log u versus log z and taking the gradient between 30 and 114 cm.

The parameter K_1 was estimated from the heat flux (when available) using

$$- \overline{\omega' T'} = K_T \, (42 \mathrm{cm}) \, \frac{\partial T}{\partial z}$$

where $\frac{\partial T}{\partial z}$ is approximated by

$$\frac{T(0,60) - T(0,30)}{60 - 30} \quad .$$

Under neutral conditions, assuming $K_T = K_m$, the formula $K_T = ku_* z$ gives a value for K_1. This approximation has been used to obtain an estimate of K_1 for experiments during which the heat flux was unavailable, but it must be remembered that values given by the shear stress meter for u_* are not highly accurate (see Section 6.4).

Table 7-5 lists the data available for diffusivity calculations, the diffusivities, and the wind profile parameters. Accurate measurements of both temperature gradient and heat flux are required for an accurate measure of the diffusivity. Thus only in experiments 2 and 5 is the diffusivity regarded as accurate. In experiment 1 the flux is small and counter-gradient, while in experiment 6 the temperature gradient is not accurate.

	Experiment Number					
	1	2	3	4	5	6
T(0,60)-T(0,30)	+0.17(.02)	-1.30(0.10)	-0.17(.06)	-0.13(.09)	+0.11(.04)	+0.08(.06)
$\overline{w'T'}$ (°K cm s^{-1})	+0.94	+38.0	n/a	n/a	-2.6	-2.8
K_1 (cm^2 s^{-1}) (flux/grad. est.)	130	670			420	830
K_1 (cm^2 s^{-1}) (ku_*z est.)	310	660	600	550	590	460
m	0.28	0.25	0.30	0.25	0.24	0.25
u_1	195	213	185	156	165	147
u_1/K_1	1.5	0.32	0.31	0.28	0.39	0.18

Table 7-5. Wind and Diffusivity Parameters for Input to RPB Model.

7.3 Comparison of Observed Temperature-Profile Modification with the Rider, Philip, and Bradley Model

ΔT_o, the change in surface temperature, was not measured. In order to compare the model with the experimental results without the necessity of supplying an arbitrary value of ΔT_o, the following shape factor was defined:

$$R_{exp} = \frac{[T(x,z_i)-T(x,z_1)]_{exp} - [T(0,z_i)-T(0,z_1)]_{exp}}{[T(x,z_2)-T(x,z_1)]_{exp} - [T(0,z_2)-T(0,z_1)]_{exp}}$$

where $z_2 > z_i > z_1$. The model can be used to predict values of this shape factor. Define

$$F(x,z) = \left(1 - I\left(\eta_T, -\frac{1+m}{1+2m}\right)\right) . \qquad (7.3.1)$$

Then

$$R_m = \frac{F(x,z_i) - F(x,z_1)}{F(x,z_2) - F(x,z_1)}$$

$$= \frac{[T(x,z_i)-T(x,z_1)]_m - [T(0,z_i)-T(0,z_1)]_m}{[T(x,z_2)-T(x,z_1)]_m - [T(0,z_2)-T(0,z_1)]_m} .$$

The shape factor, model or experimental, can be interpreted physically by the following rearrangement:

$$R = \frac{z_i - z_1}{z_2 - z_1} \times \frac{\left(\dfrac{T(x,z_i)-T(x,z_1)}{z_i - z_1}\right) - \left(\dfrac{T(0,z_i)-T(0,z_1)}{z_i - z_1}\right)}{\left(\dfrac{T(x,z_2)-T(x,z_1)}{z_2 - z_1}\right) - \left(\dfrac{T(0,z_2)-T(0,z_1)}{z_2 - z_1}\right)}$$

where $z_2 > z_i > z_1$. Hence the larger the value of R, the larger

is the temperature-gradient stabilisation in the lower layer with respect to the overall stabilisation through the deeper layer.

For each experiment the F(x,z) were calculated using the appropriate values of u_1,m, and K_1 (see Table7-6) in the formula given by Philip, (3.3.5).With the results of these calculations it is possible to compare the experimental and model shape factor values. Comparison by means of the shape factors solves the problem that neither the change in surface temperature nor (in experiments 1 and 2) the horizontal changes in air temperature are available.

Table 7-6 gives, for each experiment, the experimental shape factor and its uncertainty at the 95% confidence level, versus model prediction. Fig. 7-5 shows a plot of model and experimental shape factor values for all experiments.

The values of K_1 used as input to the model were those calculated from the heat fluxes, except for experiments 3 and 4, in which cases they were the values given by ku_*z .

It can be seen that in all cases where the upstream temperature profile is stable (experiments 1, 5, 6) the model shape factor values exceed the experimental values, while the opposite is true when the upstream temperature profile is unstable (experiments 2, 3, 4). However, there are significant differences at the 95% confidence level only in experiments 1 and 2. In the case

Expt.	Fetch (cm)	Height (cm)	R_{exp}	R_m
1	1000	60	0.39±0.14	0.80
		80	0.52±0.18	0.95
		120	0.67±0.22	0.99
		160	0.77±0.23	1.00
1	2000	60	0.42±0.11	0.65
		80	0.58±0.21	0.83
		120	0.71±0.23	0.96
		240	0.79±0.23	1.00
2	600	40	0.59±0.33	0.26
		60	0.93±0.35	0.58
		80	1.05±0.33	0.77
		120	1.09±0.31	0.95
2	1500	40	0.46±0.22	0.19
		60	0.76±0.24	0.46
		80	0.89±0.23	0.64
		120	1.00±0.25	0.87
3	1100	40	0.32±0.34	0.20
		60	0.65±0.34	0.48
		80	0.77±0.35	0.67
		120	0.90±0.35	0.89
3	2000	40	0.27±0.25	0.15
		60	0.58±0.30	0.37
		80	0.75±0.35	0.53
		120	0.94±0.35	0.75
		160	0.96±0.35	0.88
4	1000	40	0.32±0.54	0.21
		60	0.59±0.54	0.49
		80	0.71±0.57	0.68
		120	0.85±0.60	0.89
4	2000	40	0.18±0.36	0.15
		60	0.45±0.36	0.37
		80	0.64±0.36	0.53
		120	0.82±0.36	0.73
		160	0.89±0.36	0.86
5	500	40	0.17±0.36	0.28
		60	0.31±0.36	0.66
		80	0.43±0.31	0.83
		120	0.80±0.31	0.96
6	1100	40	0.09±0.63	0.15
		60	0.19±0.54	0.36
		80	0.28±0.40	0.52
		120	0.59±0.40	0.71

Table 7-6. Experimental and Model Shape Factor.

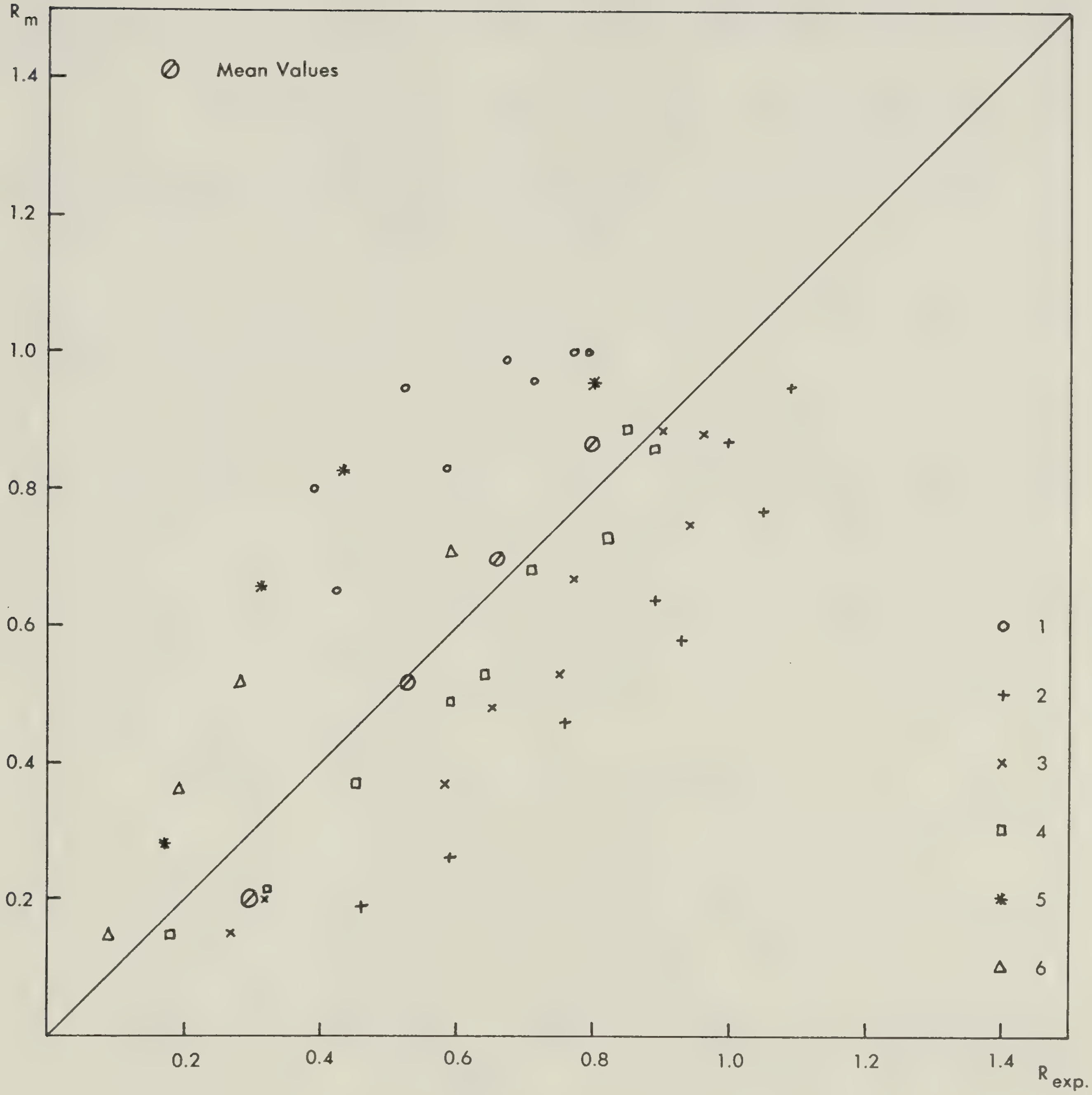

Figure 7-5. Experimental and Model Shape Factor.

of experiment 1 the diffusivity used as input to the RPB model is suspect. A larger value would seem more reasonable, and it is later shown that a larger value would give a better fit of the model and experimental shape factor values.

It thus appears that the model overestimates the shape factor in stable stratification and underestimates the shape factor in unstable stratification , but the accuracy of the shape factor and diffusivity data is not sufficient to test this hypothesis stringently.

The model values of the shape factor are dependent upon the value of u_1/K_1. Fig. 7-6 gives a family of modification curves with different values of u_1/K_1, but all for x=10 m, m=0.26. The quantity plotted to represent model modification is $F(x,z)$, defined by (7.3.1) and related to the modification because

$$T(x,z) - T(0,z) = \Delta T_0 \times F(x,z) .$$

It can be seen that as u_1/K_1 is increased

(i) the height of the IBL decreases and the difference between downstream and upstream temperature at any height is reduced. These effects are intuitively expected as windspeed increases or diffusivity decreases.

(ii) the value of

$$\frac{F(10,60) - F(10,30)}{F(10,240) - F(10,30)}$$

which is simply a model shape factor as previously

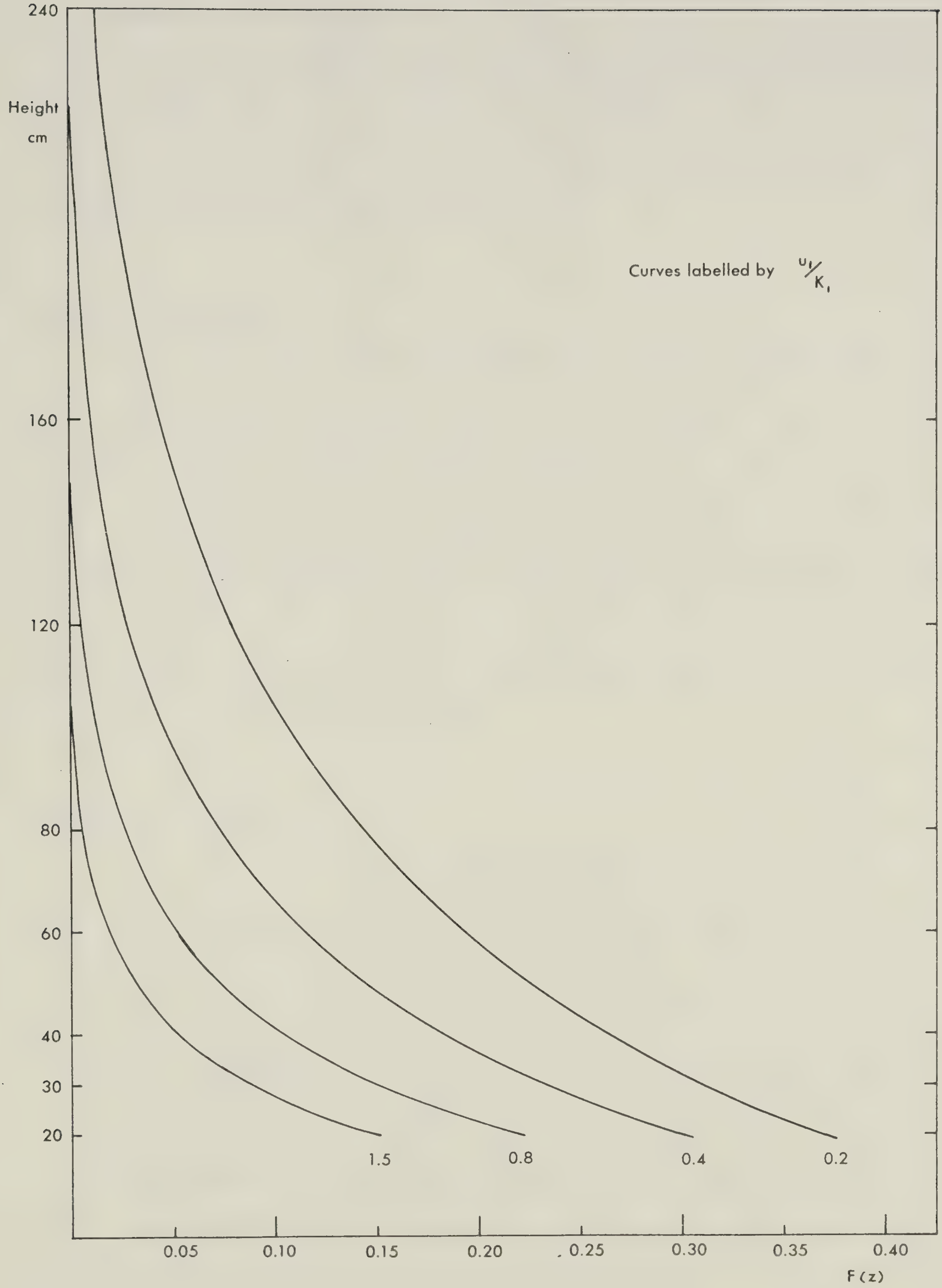

Figure 7-6. Model Modification versus u_1/K_1.

defined, increases.

It is evident that the larger the value of u_1/K_1, the larger will be the model shape factor values; i.e. the stronger will be the stabilisation in the lower layers with respect to that in the deeper layer.

STABLE UPSTREAM

The RPB model predicts excessive stabilisation in the lower layers, $R_m > R_{exp}$. If a larger value of K_1 was used in the model, the shape factors would agree more closely, but upstream-downstream temperature differences and the height of the IBL would also be affected. In addition, one would expect the value of K_1 over the cooler surface to be smaller than that measured upstream, so that the use of a larger K_1 cannot be justified.

UNSTABLE UPSTREAM

The RPB model underpredicts the stabilisation in the lower layers, $R_m < R_{exp}$. There is some justification for the use of a smaller value of K_1, because the diffusivity over the cooler surface is expected to be lower than that upstream. However, a decrease of K_1 from 670 to 150 $cm^2\ s^{-1}$ is necessary to match R_m and R_{exp} in the case of experiment 2. This seems an excessive decrease, and would result in a very low height of the model IBL, as well as small upstream-downstream temperature differences.

The experimental and model shape factors for each

height were averaged over all experiments, with the data from both masts being combined. The average values were found to be:

Height (cm)	R_{exp}	R_m
40	0.30±0.14	0.20
60	0.53±0.11	0.52
80	0.66±0.11	0.70
120	0.80±0.12	0.87

These values are plotted in Fig. 7-5. Uncertainties are at the 95% confidence level. There is no significant difference between experimental and model average shape factor.

7.4 Comparison of Model and Experimental Stabilisation

In Section 7.1 a temperature-gradient stabilisation parameter has been defined and discussed. The RPB model can be used to predict values of this parameter:

$$S_m\left(x, \sqrt{z_1 z_2}\right) = \left[\frac{T(x,z_2) - T(x,z_1)}{z_2 - z_1}\right]_m - \left[\frac{T(0,z_2) - T(0,z_1)}{z_2 - z_1}\right]_m$$

$$= \frac{\Delta T_0}{z_2 - z_1} \times \left[F(x,z_2) - F(x,z_1)\right]$$

where F is defined by (7.3.1).

Because ΔT_0 was not measured, it was decided not to attempt experiment by case-by-case model-experimental comparison of this parameter, but rather to compare mean

curves. The model average curve for stabilisation versus height was calculated by calculating the values of $F(x,z_2)-F(x,z_1)$ for each experiment, using the appropriate values of u_1, K_1, m, and x, (see Section 7.2), then averaging over all experiments to obtain a mean value for each height. The values obtained are given in Table 7-7, and apply at the mean fetch, 13 m.

z (cm)	$\frac{F(z_2) - F(z_1)}{z_2 - z_1}$
170	-0.05
113	-0.09
85	-0.14
57	-0.26
42	-0.37

Table 7-7. Mean Values of $\frac{F(z_2) - F(z_1)}{z_2 - z_1}$.

Now if a value of ΔT_0 is chosen, mean model stabilisation may be compared with the experimental mean stabilisation. Fig. 7-7 compares model and experimental stabilisation for $\Delta T_0 = -2°C$ and $\Delta T_0 = -4°C$. The shape of the model curve is quite close to that of the experimental curve. In view of the uncertainty in the experimental curve, the model curve for $\Delta T_0 = -2°C$ does not differ

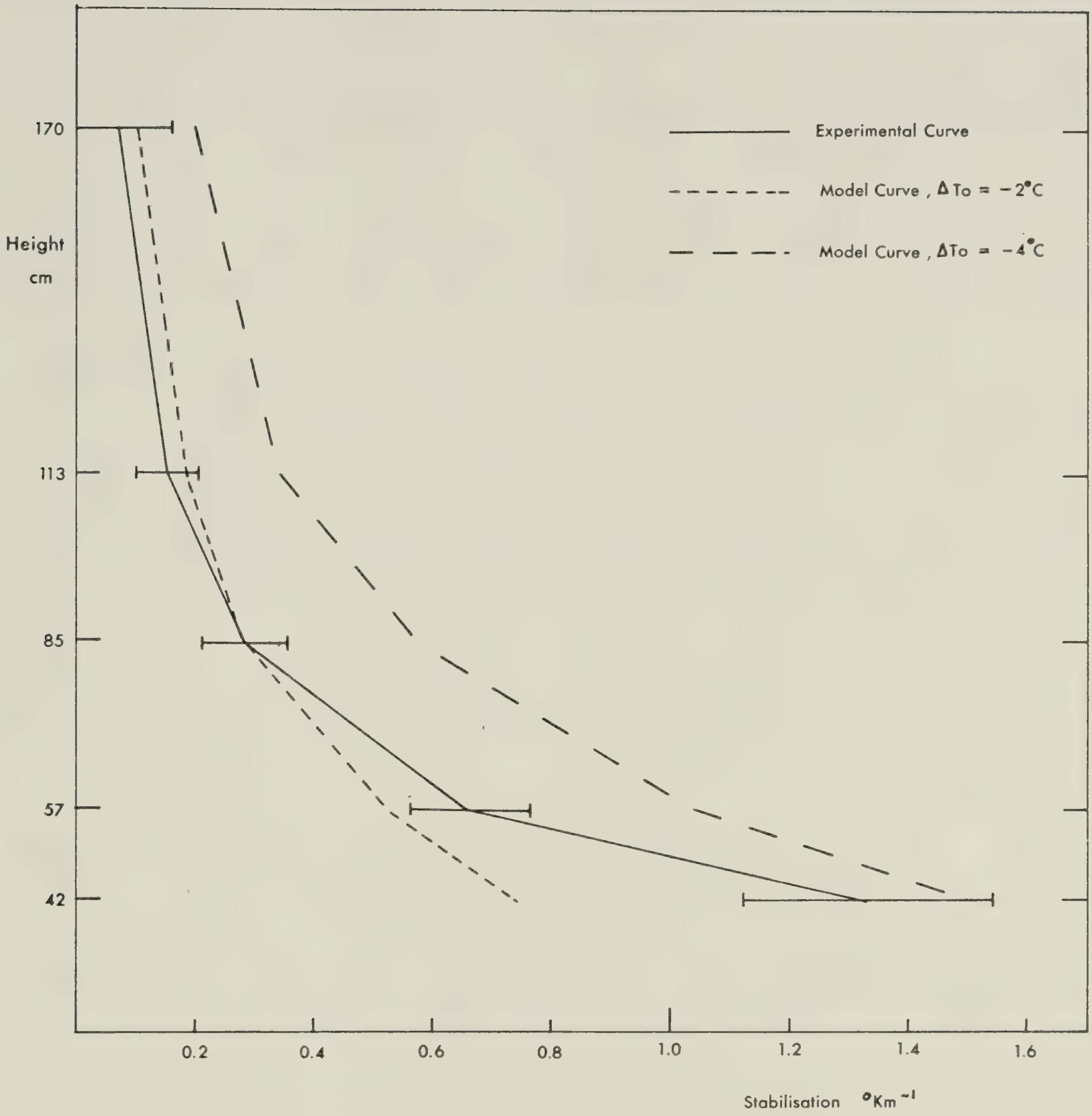

Figure 7-7. Model and Experimental Mean Stabilisation.

significantly except at the lowest two levels. As has been discussed in Section 7.3, the model overpredicts the stabilisation at low levels with respect to the overall stabilisation when the upstream flow is stable, and vice versa when the upstream flow is unstable. In the formation of a mean model curve, there has probably been some cancelling out of the over- and underprediction in individual cases, but the mean model curve nevertheless underpredicts the stabilisation in the lowest layers.

The model curve may be shifted to larger or smaller values of the stabilisation by choice of ΔT_0. In order that the mean curve should reproduce the greatest value of stabilisation observed at the lowest level, that of experiment 2 (net radiation 49 mW cm^{-2}) the value $\Delta T_0 = -9°C$ is required. To reproduce the minimum lowest level stabilisation, that of experiment 6 (net radiation 3 mW cm^{-2}), the value $\Delta T_0 = -0.5°C$ is required.

Thus the model mean curve indicates that throughout the six experiments the change in surface temperature at the leading edge varied between -0.5°C and -9°C.

CHAPTER 8

MODIFICATION OF THE VELOCITY PROFILE AND THE RADIATIVE FLUX

8.1 Experimental Wind Profiles

The numerical model of Taylor (see Section 4.1) predicted that the velocity profile would be relatively insensitive to a step change in surface temperature. For example, for a very large step in temperature the velocity modification predicted is:

Z (cm)	2	20	200
Δu (m s^{-1})	0.3	0.4	0.1

These numbers are taken from a graph given by Taylor (1970), and apply to the case

$$\Delta T_o = +75°C$$

$$x = 10 \text{ to } 20 \text{ m}$$

given that $u_* = 0.44$ m s^{-1}, the average value of u_* observed in the Ellerslie experiment, and $z_o = 1$ to 2 cm, the roughness length of the Ellerslie site. The maximum windspeed modification occurs in the range of heights 20 to 40 cm, although this can only be estimated roughly from Taylor's graph.

An attempt was made in the Ellerslie experiment to

test for velocity-profile modification and compare it with that predicted by the Taylor model.

As mentioned in Section 6.8, wind profiles were measured continuously on the 6 m upstream tower, enabling construction of a record of the upstream wind profile. The anemometers used on the upstream tower were 'Rimco' metal-cup anemometers, calibrated to C.S.I.R.O. Standards.

Downstream wind profiles were measured using 'Rimco' mini-cup anemometers. The calibration of these anemometers was inaccurate below about 1.2 m s^{-1}, but only rarely were such speeds encountered.

Possible sources of error in the wind profile data are the following:

(i) Imprecise calibration of the downwind anemometers.

(ii) Use of different anemometers upstream and downstream.

(iii) The interpolation required by the fact that upwind and downwind profiles were not measured simultaneously.

Table 8-1 gives the wind profile data, the upstream profiles being interpolated from the continuous record to give values at the times of the downwind profiles.

(i) 7th August

The trend in upstream windspeed, (a steady decrease), was duplicated downstream. Both the 1410-1420 and the 1424-1434 runs indicated that windspeed decreased

FETCH	HEIGHT (cm)	7Aug 1410 -1420	7Aug 1424 -1434	14Aug 1322 -1336	14Aug 1339 -1349	26Aug 1631 -1631	26Aug 1634 -1642	26Aug 1647 -1657	26Aug 1659 -1709	26Aug 1814 -1824	26Aug 1828 -1838	26Aug 1840 -1850	26Aug 1852 -1902	26Aug 1904 -1914
	469	4.0	2.8	3.5	3.6	3.7	3.6	3.3	2.9	3.2	3.4	3.0	2.9	2.9
	233	3.7	2.6	3.1	3.1	3.4	3.2	3.0	2.6	2.9	3.1	2.7	2.6	2.6
0	114	3.3	2.4	2.9	3.0	2.9	2.7	2.4	2.2	2.4	2.5	2.2	2.1	2.1
	54	2.8	2.0	2.4	2.4	2.3	2.2	2.0	1.8	1.9	2.1	1.7	1.7	1.7
	30	2.3	1.6	2.1	2.2	1.9	1.8	1.7	1.6	1.7	1.8	1.5	1.5	1.5
	134	3.2	2.4											
	94			2.8	2.6	2.7	2.5	2.5	2.4	1.7	2.6	2.0	2.1	2.1
A	74	2.8	2.1											
	54			2.4	2.2	2.2	2.1	2.0	1.9	1.5	2.2	1.6	1.7	1.8
	44	2.5	1.8											
	34			2.0	1.9	1.8	1.7	1.7	1.6	1.3	1.8	1.4		
	134	2.9	2.2			2.8	2.6	2.6	2.5	1.9	2.7	2.2	2.2	2.2
B	94			2.6	2.5									
	44	2.0	1.5			2.1	1.9		1.8	1.4	2.1	1.6	1.5	1.6
	34			1.9	1.8									
A,B (m)		10,20	10,20	5,15	5,15	10,20	10,20	5,15	5,15	10,20	5,15	5,15	10,20	10,20

Table 8-1. Upstream and Downstream Wind Profiles (m s^{-1}).
(uncertainties ±0.05 m s^{-1})

significantly at all heights with increasing fetch over the cool surface. The average decrease over the 10 m between the two downstream masts was 0.3 m s^{-1}. The average decrease over the 10 m between the upstream and the first downstream mast was approximately 0.14 m s^{-1}.

(ii) 14th August

From 1326 to 1350 the upstream windspeed increased slightly, by an average of 0.1 m s^{-1} over all heights. The windspeed during the 1339-1349 downstream run was an average of 0.14 m s^{-1} lower than during the 1322-1336 run. Thus the upstream trend in windspeed was not duplicated downstream. No explanation for this has been found.

During the 1322-1336 run there was a significant difference in windspeed between the 5 m and 15 m downstream masts at all heights, the speeds on the 15 m mast being lower by an average of 0.15 m s^{-1}. The upstream windspeed was lower, though not significantly, than on the 5 m mast for $z \geq 45$ cm, but was higher than on the 15 m mast for all levels. This suggests that the interpolation for upstream windspeed may have given too low a value.

During the 1339-1349 run windspeeds on the 5 m mast were significantly lower than the interpolated values on the upstream mast, with the average value of the decrease being 0.25 m s^{-1}. Windspeeds on the 15 m mast were lower than on the 5 m mast by an average of 0.1 m s^{-1}, not significant considering the uncertainties.

(iii) 26th August

During the 1623-1631 and 1634-1642 runs windspeed on the first downstream mast was significantly lower than on the upstream mast below about 50 cm. At greater heights the difference was not significant. Windspeeds on the two downstream masts did not differ significantly.

During the 1647-1657 run the top anemometer on the first downstream mast indicated a significant increase in windspeed in comparison with the interpolated upstream profile. At other levels, the differences were not significant.

During the 1659-1709 run windspeeds on the downstream masts did not differ significantly. However the upstream (interpolated) windspeed was significantly lower than downstream for heights above about 60 cm.

For the remainder of the afternoon of 26th August windspeed was variable, and the accuracy of the interpolations for upstream windspeed is dubious. In three of the five remaining runs windspeed downstream was higher than that upstream.

Because the velocity-profile modification varied considerably from run to run, it was decided to average the deceleration at each height over all runs, putting together the data on the two downstream masts. The resulting average deceleration curve is shown in Fig. 8-1. The error bars

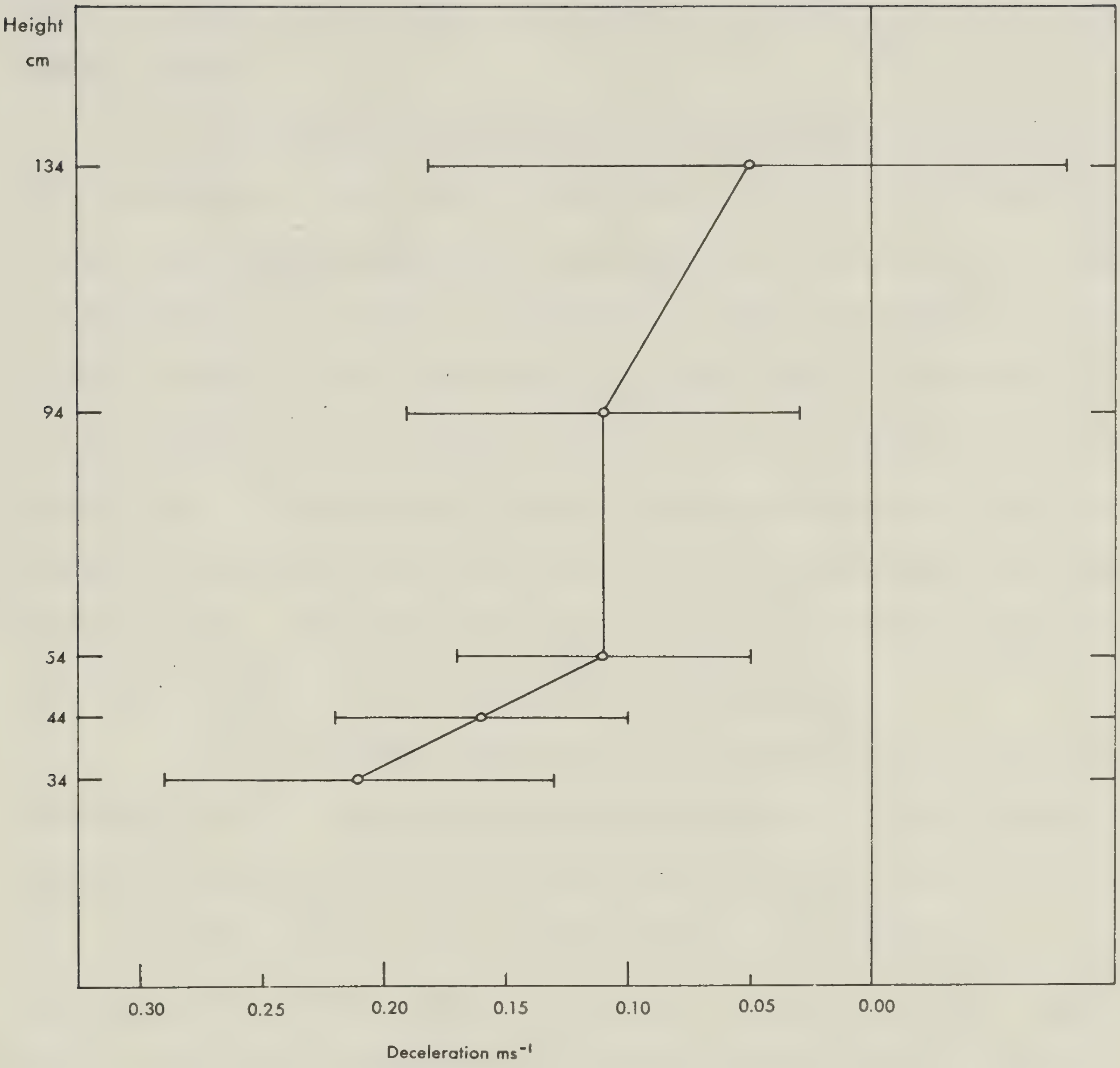

Figure 8-1. Average Deceleration over the Cool Surface.

given are at the 95% confidence level and were calculated using a paired t-test. Significant deceleration over the cool grass is indicated, for heights less than about 1 m. Because windspeed at ground (zero) cannot be modified, the maximum modification must have occurred between 35 cm and ground level.

The magnitude of the observed average deceleration is inconsistent with the Taylor model, which indicates that a very large temperature discontinuity is necessary to give a significant change in windspeed. The observed height of maximum deceleration does agree with the model estimate of 20 to 40 cm for fetches of 10 to 20 m. Because of the possibility of systematic error in the wind profile data, no definite decision can be made as to the accuracy of the Taylor model. However, it can be tentatively concluded that the model underestimates velocity modification.

A decreased horizontal windspeed over the cool grass implies by continuity the presence of a mean upward vertical velocity, or a mean difluence of the airflow around the irrigated area, or both of these possibilities. The existence of a mean upward vertical velocity would give large vertical fluxes. For example, consider the decrease in horizontal windspeed to be compensated for solely by a vertical component of windspeed over the wet grass. Using a value for the deceleration of -0.2 m s^{-1} in 10 m for all heights in the layer from 134 to 44 cm, the mean vertical velocity in the layer is of the order of 1 cm s^{-1}. Such a

vertical velocity leads to a sensible heat flux of approximately 300 mW cm^{-2} over the wet grass, and would also lead to a very large latent heat flux, depending on the absolute humidity above the grass. Hence the evaporation rate near the leading edge may be very large.

8.2 A Simple View of Wind-Profile Modification

On the 7th August both wind profile experiments displayed significantly decreasing windspeed with increasing fetch over the cool surface. Particular confidence is held in these two experiments because of the consistency in the upstream and downstream windspeed trends. In addition, significant deceleration is indicated in the average over all experiments. That windspeed modification should be observed at all can be understood by the simple hypothesis that as the air passing over the cool surface becomes more stably stratified, mixing of momentum from higher levels becomes less efficient. However, the question is raised, 'is it theoretically possible to have a difference in windspeed between the dry and the wet (cool) grass of the order of 0.2 m s^{-1} ?'.

An approach to answering this question is to choose a velocity-profile formula which incorporates stability effects and to see what velocity change is given by a change in stability. It must be remembered, however, that wind profile formulas are constructed using data gathered at sites where horizontally uniform and steady

conditions prevail, and that they are really only intended to be applied in such situations.

The change in stability (i.e. change in L, the Monin-Obukhov length) depends on the change in the heat flux. Unfortunately, no estimate of this can be made for the 7th August, when the heat flux upstream was small and counter-gradient. However an estimate of the change in stability can be made for the 14th August, on which day decreased windspeed over the cool grass was also observed although confidence in the accuracy is less.

On the 14th August the temperature profile was unstable both upstream and downstream. Businger (1973) gave the following expression for the wind profile in unstable stratification:

$$u = \frac{u_*}{k}\left[\ln\frac{z}{z_0} - 2\ln\frac{1+x}{2} - \ln\frac{1+x^2}{2} + 2\arctan\left(x+\frac{\pi}{2}\right)\right]$$

where $x = \left(1 - 15\,\frac{z+z_0}{L}\right)^{1/4}$.

A change in stability will lead to a change in u, assumed to be given approximately by

$$\Delta u = \frac{\partial u}{\partial L}\,\Delta L \quad .$$

Measurement of the upstream temperature profile and heat flux on 14th August allowed calculation of a heat diffusivity, K(30 cm) = 670 $\mathrm{cm^2\,s^{-1}}$. In order to calculate the change in the heat flux (and hence in L) the diffusivity measured upstream was used with the downstream gradient on the 15 m fetch mast to give an estimate of the downstream heat flux. Results were

$$\overline{w'T'}\ (\text{upstream}) = +0\cdot4\ ^{\circ}\text{K m s}^{-1}$$

$$\overline{w'T'}\ (\text{downstream}) = +0\cdot1\ ^{\circ}\text{K m s}^{-1} .$$

For a height of 60 cm, the change in windspeed from upstream to downstream given by this simple method is

$$u(\text{downstream}) - u(\text{upstream}) = -0.1 \text{ m s}^{-1}$$

Windspeed modification of this order of magnitude was observed on the 14th August. It thus seems possible that the considerable velocity-profile modification indicated in some of the Ellerslie experiments did occur, and that the Taylor model underestimates such modification.

8.3 Modification of the Net Radiative Flux

In none of the experiments was a significant difference shown in the mean net radiation between the wet and the dry surfaces, but in all cases the (insignificant) change was such that the net radiation was increased over the wet surface; for example

(i)	Experiment 2	50.2±0.8 mW cm^{-2} (wet)
		48.7±0.8 mW cm^{-2} (dry)
(ii)	Experiment 4	16.2±0.8 mW $c,^{-2}$ (wet)
		14.8±0.8 mW cm^{-2} (dry

However just prior to experiment 2 when a net radiometer was moved from dry to wet grass its output jumped by 4.4±1.5 mW cm^{-2}, indicating a significant increase in the net radiation over the wet grass.

The net radiation can be written

$$R_n = (1-r)R_s + R_a - \epsilon\sigma T_o^4 \quad .$$

The materials comprising the earth's surface have emissivity values very close to 1.00 (see Gates (1965)). Typical values are:

plants	0.97
soils	0.95-0.98
snow	0.98-0.995 .

If a change in the emissivity was supposed to have caused the observed change in the net radiation between the wet and the dry ground, then the change in emissivity required is given by

$$\Delta\epsilon = \frac{\Delta R_n}{\sigma T_o^4} \quad .$$

Values of ΔR_n and ϵ using T_o =290°K are:

$\Delta\epsilon$	0.01	0.05	0.1	0.5
ΔR_n (mW cm^{-2})	0.4	2.0	4.0	20.2

On the basis of these numbers, it seems unlikely that a change in the emissivity lead to the change in the net radiation.

It is generally assumed that horizontal changes in R_a and R_s are negligible for a small irrigated area. However there was possibly a change in the reflectivity, r. Kuhn and Suomi (1958) tabulate measured values of r over wet and dry grass, but there is so much variability in the numbers given that no conclusion can be made.

The simplest explanation for the observed change in the net radiation is the change in surface temperature. A change in surface temperature gives the following change in the net radiation:

$$\Delta R_n = - 4 \epsilon \sigma T_o^3 \Delta T_o \ .$$

Values of ΔR_n for given ΔT_o are :

ΔT_o (°C)	-1	-2	-5	-10	-20
ΔR_n (mW cm^{-2})	0.5	1.1	2.7	5.4	10.8

It was found that a change in surface temperature of about -9°C is required to match the RPB mean stabilisation to that observed during experiment 2 at 30 cm (see Section 7.4). As can be seen from the numbers above, such a change would give a change in the net radiation of approximately the size observed.

CHAPTER 9

CONCLUSION

9.1 Summary of Findings

The local advection model of Philip (1959) has been compared with an extension of an approximate solution due to Shwetz (1949) for the artificial problem of 'θ-less' upstream flow encountering a step change at the surface from $\theta=0$ to $\theta=1$. The two methods were found to give similar predictions for the growth of the IBL. The Shwetz solution leads to a simple expression, Eq. (3.7.1), for the height of the IBL as a function of fetch.

From the six temperature-profile modification experiments analysed, mean results have been given for the cooling and the stabilisation of the temperature gradient over the wet grass. No significant difference was found between the cooling on the two downstream masts (separated by 10 m) but at the lowest level, 30 cm, cooling was significantly stronger under unstable conditions than under stable conditions. Greatest stabilisation of the temperature-gradient occurred in the lowest layers considered.

The Rider, Philip, and Bradley (1963) model of temperature-profile modification has been compared with the

experimental data of the Ellerslie experiment without the necessity of estimation of ΔT_0, the change in surface temperature, by definition of a shape factor (see Section 7.3). Confidence intervals for the experimental data are wide, and significant differences between model and experimental shape factors were observed in only two experiments. A tentative conclusion is that the RPB model overestimates stabilisation in the lowest layers with respect to that over a deeper layer in stable conditions, and vice versa in unstable conditions. The shape factors were averaged over all experiments, and there was found to no significant difference between the model and experimental values.

The model curve for mean stabilisation , with a step in temperature of -2°C, compares well with the observed stabilisation except below about 60 cm, where stabilisation is underestimated. The model curve indicates that the range of values of ΔT_0 in the six experiments was -0.5 to -9°C.

Significant deceleration in the mean windspeed over the cool grass was observed in the average over 13 wind-profile experiments. The deceleration was stronger than that predicted by the numerical model of Taylor (1970), but maximum deceleration occurred at approximately the height predicted by the model.

9.2 Recommendations

The following comments are intended to convey to possible future experimenters the lessons learned in the Ellerslie temperature-profile modification experiment.

First and foremost, it is imperative that the system used to measure the mean temperature field be well tested and accurately calibrated prior to the experiment. Because the mean temperature differences are very small in comparison with turbulent fluctuations, it is impossible to obtain definitive data with an improperly prepared network. Furthermore, even a satisfactory measurement system will not provide meaningful data unless the sampling procedure conforms with the requirements of stationarity and of sufficient number of data points.

The crosswind dimension of the leading edge and modified surface should be made sufficiently large, or the downwind fetches sufficiently small, so that at the furthest downstream mast there is no possibility that the air arriving has not come across the leading edge. The site chosen must be large enough to allow this requirement to be met, and preferably large enough to allow all wind directions to be used with confidence that the upwind conditions are uniform, because the necessity of using only a subrange of wind directions may eliminate the possibility of experimentation on many otherwise satisfactory occasions.

Instruments for profile measurements should be placed at the same heights on all masts involved, in order

to facilitate comparisons. For the same reason, the period of averaging should be the same on all masts. Non-simultaneous, spatially-separated profiles may be very difficult to compare, particularly if conditions are not very steady.

In the Ellerslie experiment no significant difference was observed between the average cooling on each of the downstream masts. In many cases , no significant difference was observed in windspeed between the two downstream masts. Because of this, it would seem logical to divide all available sensors between the upwind and a single downwind mast. This would be beneficial in optimising resolution (by which means it may be possible to determine the top of the IBL) and in simplifying the experimental layout.

While ensuring that all necessary variables are measured, the experimenter should keep the experiment as simple as possible, concentrating on performing the measurements with highest priority as accurately as possible. Every additional instrument used may demand pre-experimental work and planning and attention during the experiment which is better spent on the primary measurements.

If possible, upstream and downstream surface temperature should be measured, as the temperature step is usually required as input for any model.

Modification will be strongest under conditions of

strong insolation (and therefore strong evaporation). Such conditions are therefore preferable, as long as winds are not too light and variable.

In conclusion, experiments of this nature are time consuming and may be expensive. Consequently careful and unhurried planning and preparation is vital.

REFERENCES

Berntsen, L., 1971: Comparative heat flux measurements in the surface boundary layer. M.Sc. Thesis, University of Alberta.

Businger, J.A., Wyngaard, J.C., Izumi, Y., and E.F. Bradley, 1971: Flux-profile relationships in the atmospheric surface layer. J. Atmos. Sci., 28, 181-189.

Businger, J.A., 1973: Turbulent transfer in the atmospheric surface layer., in D.A. Haugen (ed.), Workshop on Micrometeorology., American Meteorological Society , 67-100.

Dyer, A.J., and T.V. Crawford, 1965: Observations of the modification of the microclimate at a leading edge. Quart. J. Roy. Meteor. Soc., 91, 345-348.

Gates, D.M., 1965: Radiant energy, its receipt and disposal. Meteorological Monographs, 6(28), 1-26.

Kaimal, J.C., and J.A. Businger, 1966: A continuous wave sonic anemometer-thermometer. J. Appl. Meteor., 2, 156-164.

Kaimal, J.C., 1975: Sensors and techniques for direct measurement of turbulent fluxes and profiles in the atmospheric surface layer. Atmospheric Technology, 7, 7-14.

Kuhn, P.M., and V.E. Suomi, 1958: Airborne observations of albedo with a beam reflector. J. Meteor., 15, 172-174.

Morgan, D.L., Pruitt, W.O., and F.J. Lourence,1971: Analysis of energy, momentum, and mass transfers above vegetative surfaces. U.S. Army Electronics Command Research and Development Technical Report, ECOM

68-G10-F.

Novikova, S.P.,1969: On the problem of transformation of the meteorological elements. Meteorologia I Gidrologia, 12, 89-93.

Panchev, S., Donev, E., and N. Godev, 1971: Wind profile and vertical motions above an abrupt change in surface roughness. Bound.-Layer Meteor., 2, 52-63.

Philip, J.R., 1959: The theory of local advection: I. J. Meteor., 16, 535-547.

Plate, E.J.,1971: Aerodynamic characteristics of atmospheric boundary layers. United States Atomic Energy Commission, Critical Review Series.

Rider, N.E., Philip, J.R., and E.F. Bradley, 1963: The horizontal transport of heat and moisture-a micrometeorological study. Quart. J. Roy. Meteor. Soc., 89, 507-531.

____, ____, and ____, 1965: Horizontal transport of heat and moisture-a micrometeorological study. Discussions, Quart. J. Roy. Meteor. Soc., 91, 236-242.

Sutton, O.G., 1953: Micrometeorology. McGraw-Hill Book Company Inc.

Shwetz, M.E., 1949: On the approximate solution of some boundary-layer problems. Appl. Mathematics Mech., 13(3), (Moscow).

Taylor, P.A., 1970: A model of airflow above changes in surface heat flux, temperature and roughness for neutral and unstable conditions. Bound.-Layer Meteor., 1, 18-39.

____, 1970: Airflow above changes in surface heat flux, temperature and roughness;an extension to include the stable case. Bound.-Layer Meteor., 1, 474-497.

Vries, D.A. De, 1959 : The influence of irrigation on the energy balance and the climate near the ground. J. Meteor., 16, 256-270.

Weisman, R.N., 1975: A developing boundary layer over an evaporating surface. Bound.-Layer Meteor., 8, 437-445.

Wesely, M.L., Thurtell, G.W., and C.B. Tanner, 1969: A fast-response thermometer for eddy correlation measurements. U.S. Army Electronics Command Research and Development Technical Report, ECOM 66-G22-F., 61-72.

Wyngaard, J.C., Cote, O.R., and Y. Izumi, 1971: Local free convection, similarity, and the budgets of shear stress and heat flux. J. Atmos. Sci., 28, 1171-1182.

Yih, C.-S., 1952: On a differential equation of atmospheric diffusion. Trans. Amer. Geophys. Union, 33, 8-12.

APPENDIX

NOMENCLATURE

A	Sensible heat exchange between surface and air, positive upward; (mW cm^{-2}).
c_p	Specific heat at constant pressure; (cal g^{-1} $^{o}K^{-1}$).
c_v	Specific heat at constant volume; (cal g^{-1} $^{o}K^{-1}$).
E	Evaporation rate, positive upward; (cm s^{-1}).
e	Absolute humidity; (g cm^{-3}).
e_s	Absolute humidity at saturation; (g cm^{-3}).
e_o	Surface absolute humidity upwind of discontinuity; (g cm^{-3}).
e_1	Surface absolute humidity downwind of discontinuity; (g cm^{-3}).
Δe_o	Change in surface absolute humidity $(e_1 - e_o)$; (g cm^{-3}).
F	Dimensionless function defined by equation (7.3.1).
G	Soil heat flux density at the surface, positive upward; (mW cm^{-2}).
g	Acceleration of gravity; (cm s^{-2}).

I	Incomplete gamma function ratio; (dimensionless).
K_e	Eddy diffusivity for water vapour; $(\mathrm{cm}^2\ \mathrm{s}^{-1})$.
K_T	Eddy diffusivity for heat; $(\mathrm{cm}^2\ \mathrm{s}^{-1})$.
K_m	Eddy diffusivity for momentum; $(\mathrm{cm}^2\ \mathrm{s}^{-1})$.
K_1	Reference value of diffusivity in power-law expression for diffusivity; $(\mathrm{cm}^2\ \mathrm{s}^{-1})$.
k	von Karman's constant (0.4); also used for thermal conductivity.
$\underset{\sim}{\hat{k}}$	Unit vector in vertical (z) direction.
L	Latent heat of evaporation of water, $(585\ \mathrm{cal}\ \mathrm{g}^{-1})$;also used for Monin-Obukhov stability length in Chapter 4.
m	Exponent in power law for wind profile; (dimensionless).
n	Exponent in power law for diffusivity profile; (dimensionless).
p	Pressure.
q	Specific humidity; (dimensionless).
R	Gas constant; $(\mathrm{m}^2\ \mathrm{s}^{-2}\ {}^{\circ}\mathrm{K}^{-1})$.
$\mathcal{R}$	Rate of heat addition by radiation.
R_a	Flux density of longwave radiation recieved at the surface, positive downwards; $(\mathrm{mW}\ \mathrm{cm}^{-2})$.
R_s	Flux density of shortwave radiation received at the surface, positive downwards; $(\mathrm{mW}\ \mathrm{cm}^{-2})$.

R_n	Net radiation, positive downwards; (mW cm^{-2}).
r	Reflection coefficient of the surface for short wave radiation; (dimensionless).
T	Temperature; (^oK).
T_D	Dewpoint temperature; (^oK).
T_0	Surface temperature upwind of discontinuity; (^oK).
T_1	Surface temperature downwind of discontinuity; (^oK).
ΔT_0	Change in surface temperature, ($T_1 - T_0$); (^oK).
u	Windspeed in x direction; (m s^{-1}).
u_1	Reference velocity in power law for velocity-profile; (m s^{-1}).
u_*	Friction velocity; (m s^{-1}).
$\underset{\sim}{v}$	Velocity vector; (m s^{-1}).
v	Windspeed in y direction; (m s^{-1}).
w	Windspeed in z direction; (m s^{-1}).
x	Horizontal coordinate perpendicular to leading edge; (cm).
y	Horizontal coordinate parallel to leading edge; (cm).
z	Vertical coordinate; (cm).
z_1	Reference height; (cm).

α	Constant of proportionality defined in Section 6.3.
β	Constant of proportionality defined in Section 6.3.
δ	Height of IBL; (cm).
ϵ	Emissivity of surface for longwave radiation; (dimensionless).
θ_e	Equivalent temperature; ($^{\circ}$K).
θ_p	Potential temperature; ($^{\circ}$K).
ϕ	Rate of dissipation of kinetic energy into heat.
ϕ_m	Monin-Obukhov similarity function for momentum; (dimensionless).
ϕ_h	Monin-Obukhov similarity function for heat; (dimensionless).
η	Transformation defined by equation (3.3.1).
Γ_i	Incomplete gamma function; (dimensionless).
Γ	Gamma function; (dimensionless).
ρ	Density of air; (g cm^{-3}).
ρ_w	Density of liquid water; (g cm^{-3}).
σ	Stefan-Boltzman constant; (cal s^{-1} cm^{-2} $^{\circ}$K^{-4}).
ν	Kinematic viscosity.

(A prime denotes a turbulent fluctuation).

B30161